Joint Angle-Frequency Estimation for Multiple Signals with Circular Arrays

Joost Geelhoed

Master of Science Thesis

TU Delft Delft University of Technology

Circuits and Systems

Joint Angle-Frequency Estimation for Multiple Signals with Circular Arrays

Master of Science Thesis

For the degree of Master of Science in Telecommunications at Delft University of Technology

Joost Geelhoed
Thesis Number: CAS-MS-2014-03

June 17, 2014

Faculty of Electrical Engineering, Mathematics and Computer Science · Delft University of Technology

The work in this thesis was supported by TNO Defence, Safety and Security. Their cooperation is hereby gratefully acknowledged.

Delft University of Technology
Department of
Circuits and Systems

The undersigned hereby certify that they have read and recommend to the Faculty of Electrical Engineering, Mathematics and Computer Science for acceptance a thesis entitled

Joint Angle-Frequency Estimation for Multiple Signals with Circular Arrays

by

Joost Geelhoed

in partial fulfillment of the requirements for the degree of

Master of Science Telecommunications

Dated: June 17, 2014

Supervisor(s):

Prof.dr.ir. A.J. van der Veen

Ir. J.B. Punt

Reader(s):

Prof.dr. A. Yarovoy

Abstract

In electronic warfare information about radio signals is gathered. Parameters as the direction-of-arrival (DOA) and the frequency can be estimated from sampled data received on antenna arrays. The objective of this thesis is to investigate the use of circular arrays for joint angle-frequency estimation (JAFE). A 1-D (azimuth and frequency) and 2-D (azimuth, elevation and frequency) JAFE algorithm is presented. Both algorithms use phase-mode excitation and ESPRIT. The 1-D algorithm with spatial smoothing is introduced. With this algorithm it is possible to estimate signals with similar frequencies, when the elevation is the same and known for all signals of interest. Simulations demonstrate that when two signals are coherent and a spatial smoothing factor of two or higher is applied the algorithm is able to estimate the azimuth correctly. It is also demonstrated that when two signals have the same DOA a temporal smoothing factor of two is necessary and that more temporal smoothing reduces the standard deviation of the azimuth estimation. It is shown that the phase-mode excitation technique introduces a systematic error that is considerably high for few antenna elements and an even number of elements. It is demonstrated that interpolation can reduce this error in case a UCA of 5 elements, but not for a UCA of an even number of 12 elements. The sample rate used for sampling can be adjusted to the Nyquist rate or higher. Simulations demonstrate that a little bit oversampling reduces the RMSE (Root Mean Square Error) of the azimuth, elevation and frequency. It shows that after a certain point oversampling increases the RMSE error of the elevation and especially the frequency estimation. An ESPRIT-based algorithm for joint angle-frequency-delay estimation is introduced. For the delay estimation, using a matched filter approach with ESPRIT, it is possible to estimate the delay correctly for a SNR above 40 dB only, since it is very sensitive to imperfections in the signal separation.

Table of Contents

List of Figures

Chapter 1

Introduction

In wireless communication baseband data signals are modulated on a carrier frequency in order to transmit them. Since these signals are transmitted wirelessly they can be intercepted from arbitrary locations as long as the power of a particular signal is not too weak at that particular location. From intercepted signals a lot of useful information, besides the data they transfer, can be derived including the directions they are coming from, the delays of multipath rays, the frequencies and the polarizations. This information can be used for example in electronic warfare, telecommunications and geophysics. This thesis focuses on joint angle-frequency estimation (JAFE) for electronic warfare where information of signals can be used to gather as much information as possible about radio communication in an environment.

1-1 Context

To gather information about the location of some transmitter, special antennas and antenna arrays are used to find the direction of incoming signals. TNO has a demand for joint angle-frequency estimation with a circular array. The algorithm used for this estimation should be able to gather information about frequencies and directions of the radio sources in the environment.
A lot of research is done on JAFE for the uniform linear array. One drawback is that linear antenna arrays can only estimate directions from -90 degrees to 90 degrees relative to any axis perpendicular to the linear array. Circular arrays are able to estimate signals from 0 to 360 degrees in azimuth and 0 to 90 degrees in elevation. For some purposes the geometry of a circular array is more convenient than that of a linear array, for example when they must be mounted around a mast. Another advantage of uniform circular arrays is the uniform performance from all azimuth angles and the spatial symmetry between the elements which is advantageous when compensating for mutual coupling [1]. One drawback of circular arrays is that the array manifold is not of the Vandermonde form like it is for uniform linear arrays. This structure offers a lot of opportunities for signal processing, like the application of root-MUSIC (MUltiple SIgnal Classification), ESPRIT (Estimation of Signal Parameters

via Rotational Invariance Techniques) algorithm [2, 3] and the spatial smoothing technique which makes it possible to separate signals that are correlated or coherent [4].

1-2 JAFE techniques

To obtain the DOA and matching frequency of signals different methods could be used. The maximum likelihood method reaches the lower bound on the estimation variance asymptotically. In case of multiple parameter estimation the maximum likelihood estimator (MLE) requires a multidimensional optimization problem, which is computationally expensive. There is a lot of research done and going on about more efficient techniques for the estimation of signal parameters. The DOA estimators can be divided into two types of estimators: spectral-based and parametric estimators [5].

A spectrum-based estimator, like the Bartlett method or MVDR (Minimum Variance Distortionless Response), could be used for DOA estimation and when the DOAs are estimated, beamforming on the data matrix makes it possible to estimate the matching frequencies. A disadvantage is that the resolution of the DOAs is not very high. For a circular array antenna with 8 elements the half-power beamwidth is circa 21 degrees and for an array with 16 elements the half-power beamwidth is circa 10 degrees [6]. Another disadvantage is that it has sidelobes. So despite of the attenuation in directions other than the main lobe, signals outside the center of the main lobe or signals in the sidelobes can still be stronger than the signal in the direction to be estimated. In that case the frequency of the wrong signal dominates and thus a wrong result is obtained from the estimator.
When after beamforming two or more signals with different frequencies are obtained the frequency estimation results in multiple frequency estimates. Then it is not clear which frequency belongs to which signal, which is important information in some situations, for example for tracking or in case the delay between multipaths is to be estimated.
Another option is to estimate the frequency first and then use a frequency filter, to filter out the other frequency components. But, as with beamforming, the algorithm does not exactly estimate the angle-frequency couples and the algorithm does not combine the temporal and spatial information for better results.
Besides options that operate in two steps a peak-finding algorithm for a 3-D spectrum, with 2-D DOA (azimuth and elevation) and frequency, can be used. Then no beamforming or filtering is required to suppress other signals. A disadvantage is that it is computationally not efficient.
To enhance the resolution of the spectral-based estimators the singular value decomposition can be used to reduce the data matrix to the signal subspace. This is used in for example MUSIC [2]. Besides the spectral-based estimators there exist parametric estimators, like root-MUSIC [7], Matrix Pencil [8] and ESPRIT [7]. These techniques can achieve a high resolution.

In literature frequently JAFE-algorithms based on ESPRIT [9] are used. ESPRIT is an estimation technique which exploits the shift invariant structure of vectors to compute a parameterized variable, for example the delay, DOA or frequency. This is done from a signal subspace which is first obtained by performing a singular value decomposition on the data. DOA estimation in ESPRIT is based on the array geometry, which must have a shift

invariant structure. Therefore it requires accurate calibration. Usually MUSIC has a better performance than ESPRIT, but ESPRIT requires less computations [10]. ESPRIT is also more robust with respect to array imperfections than MUSIC [10]. Cherntanomwong, Takada and Tsujitested tested the ESPRIT algorithm with and without spatial smoothing in an anechoïc chamber and outside [11]. Both tests are performed with a uniform linear array and a SNR of 36 dB. The measurements show that ESPRIT is able te estimate DOAs with an estimation error below 0.5 degrees.
In 1996 an ESPRIT-based algorithm for joint 2-D-angle-frequency estimation for rectangular arrays was developed [12]. Here 2-D means that the azimuth and elevation are estimated. The data matrix is constructed with spatial and temporal samples in the vectors before estimating the signal subspace. Then the signal subspace contains orthonormal vectors from which the frequencies and DOAs can be computed. ESPRIT is only applicable when there is a Vandermonde structure, although the spacing between the antennas does not have to be uniform in case some correction is applied [13] [14].

For 2-D angle estimation the geometry has to be 2-D as well, so ESPRIT for L-shaped arrays [15] and uniform circular arrays is developed [16]. Since these arrays span a planar area they cannot distinguish from which side of the plane the signals come. In order to be able to uniquely estimate a signal's direction in three dimensions an array that spans a three dimensional area must be used, such as a spherical array [17] or concentric circular array [18]. With one or more directional antennas the ambiguity problem of the side from which the signals impinge the planar array can be solved.
This thesis concentrates on the circular array. For this type of array several possibilities for joint angle-frequency estimation exists. Some algorithms are based on beamspace transformation and some on fourth-order cumulants [19]. The technique using fourth-order cumulant matrices for DOA and frequency estimation uses three cumulant matrices: one reference matrix, one with a spatial sample shift and one with a temporal sample shift. The spatial shifted matrix is used for the estimation of the DOAs and the temporal shifted matrix is used for the estimation of the frequencies, just as in ESPRIT. An advantage of fourth-order cumulants is that they are zero for Gaussian variables. It does not matter if they are white or colored [20]. For short data blocks the result of second-order statistics is better than that of high-order statistics [21]. This thesis focuses on ESPRIT, which can only be used, but not directly, when the beamspace transform is applied.

MUSIC and ESPRIT exploit the singular value or eigenvalue decomposition to achieve a high resolution. These decompositions require the data matrix to be of a rank equal to the number of signals. When signals are coming from the same direction or have the same frequencies and and a matrix with only spatial samples in the rows and temporal samples in the columns this results in a rank deficiency. When sources are coherent or highly correlated, spatial smoothing, with or without forward-backward averaging [22], can restore the rank of the data matrix. This technique requires the Vandermonde structure [4], so it can not be directly applied to the data matrix of a uniform circular array. With phase-mode excitation the array manifold of the uniform circular array can be transformed to a virtual linear array manifold [23]. Then spatial smoothing can be applied and algorithms that require the Vandermonde structure, like root-MUSIC [24] and ESPRIT [10], can be used. This transformation of the array manifold requires knowledge of the elevation.

1-3 Problem Formulation and Thesis Outline

A.N. Lemma has investigated JAFE algorithms extensively for different array geometries and describes some solutions for the circular array geometry [3]. His work is a basis for this thesis. There is a interest at TNO in more knowledge about JAFE-algorithms for multiple signals with a circular array. In electronic warfare all types of signals can be present, for example coherent signals, signals that are coming from the same direction and signals with a signal power density below the noise level. The number of antennas that is required for the algorithm to perform well should not be too high. Fewer antennas has the advantage that it costs less and the size of the whole array can be smaller.

This thesis describes the research for the possibilities in electronic warfare with a circular array with the following characteristics:

- The algorithm estimates the right combinations of angles and frequencies of multiple signals with high resolution.
- The algorithm is applicable on a (uniform) circular array with a small number of antenna elements, preferably between 5 and 10.
- It is important that the algorithm is computationally efficient.
- The algorithm must be able to estimate the parameters of coherent signals and signals with the same DOA.
- The algorithms must be able to estimate signals with both high and low signal-to-noise ratio (SNR).

In this thesis the performance of JAFE for circular arrays [16] is investigated for a small number of antenna elements, between 5 and 20. It is shown that interpolation can improve the performance of this algorithm as an uneven number of physical antenna elements is used.

First I will introduce the data model in chapter 2. In chapter 3 a description of a transformation of the circular array geometry to a virtual linear array is given. In chapter 4 the JAFE-algorithm for 1-D (azimuth) and 2-D DOA (azimuth and elevation) estimation is described. These algorithms are evaluated in chapter 5. The singular value decomposition is used to obtain a high resolution. A common problem of DOA and frequency estimation when the singular value decomposition is used is that the performance deteriorates when the DOAs or carrier frequencies of two or more signals come close together. Some extra possibilities of the algorithm are described in chapter 8.

Chapter 2

The Data Model

To find a good data model the transmitter, channel and receiver must be taken into account.

Transmitter: data are generated by an information source and in case of a digital transmitter the source produces a bit stream which is modulated according to a certain modulation scheme. This baseband signal $\bar{s}(t)$ is transformed to a passband signal, $r(t)$ by putting the data symbols on a certain carrier frequency or frequencies. Information is carried in the frequency, phase and/or amplitude of the signal.

Channel: once the signal is generated it is transmitted over a wireless channel. The signal reflects, attenuates, etc. Furthermore there are other signals causing interference and there are sources causing noise, like radiation from electronics.

Receiver: signals are received by an antenna or antenna array. The analogue signal is sampled and quantized and some signal processing like beamforming and demodulation takes place in the receiver.

A simplified data model is used for the described algorithms and simulations. Section 2-1 describes the narrowband assumption, section 2-2 describes the array manifold of the uniform circular array and section 2-3 describes the received signal representation.

2-1 Narrowband Signals

In case of narrowband signals the bandwidth B of the observed band is much higher than the bandwidth W of the signals in it. This is depicted in figure 2-1. This implies that the baseband signals do not change over small time delays and time delays can thus be translated to a phase shift [3]. The narrowband assumption also states that the center frequency f_c of the observed band is much higher than the bandwidth of the observed band B, which implies that all signals in that band have the same phase shifts for a certain time delay [3]. This can be clarified with the following equations.

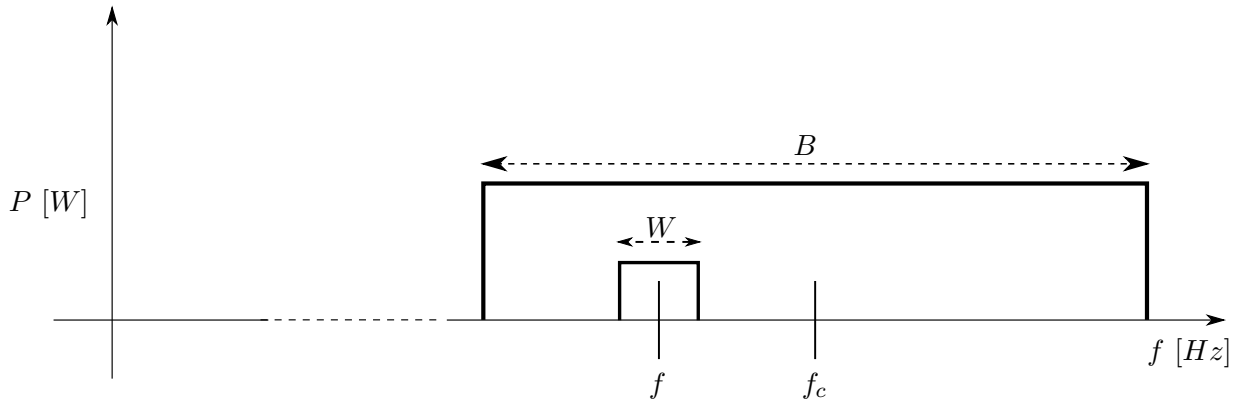

Figure 2-1: Narrowband signal in observed band

The received signal $s(t)$ be represented as follows:

$$s(t) = \bar{s}(t)e^{j2\pi f_c t} \tag{2-1}$$

where $\bar{s}$ is the complex envelope of the signal $s(t)$ (see section 2-3), also called the baseband signal. When the narrowband assumption holds true the baseband signal does not change over small time delays τ:

$$\bar{s}(t-\tau) \approx \bar{s}(t) \tag{2-2}$$

This is true if $|2\pi W\tau| \ll 1$. Then a delay in the received signal $s(t)$ causes a phase shift determined by the frequency of the signal which is approximately the same as the center frequency of the observed band B according to the narrowband assumption:

$$s(t-\tau) = \bar{s}(t-\tau)e^{j2\pi f_c(t-\tau)} \approx \bar{s}(t)e^{j2\pi f_c(t-\tau)} = s(t)e^{-j2\pi f_c\tau} \tag{2-3}$$

2-2 Uniform Circular Array Geometry

All antennas are assumed to be isotropic antennas, which is only possible in theory. In a uniform circular antenna array all M antennas are equally spaced from each other and distributed in a circle as in figure 2-2.

The linear spacing between the antenna elements is related to the radius. The relation between the radius r and the spacing d between the elements can easily be derived and is given in the following equation:

$$d = 2r\sin(\frac{\pi}{M}) \tag{2-4}$$

where d and r are measured in fractions of the signal wavelength. Spacing d is the length of the straight line between two elements. The second statement about narrowband signals

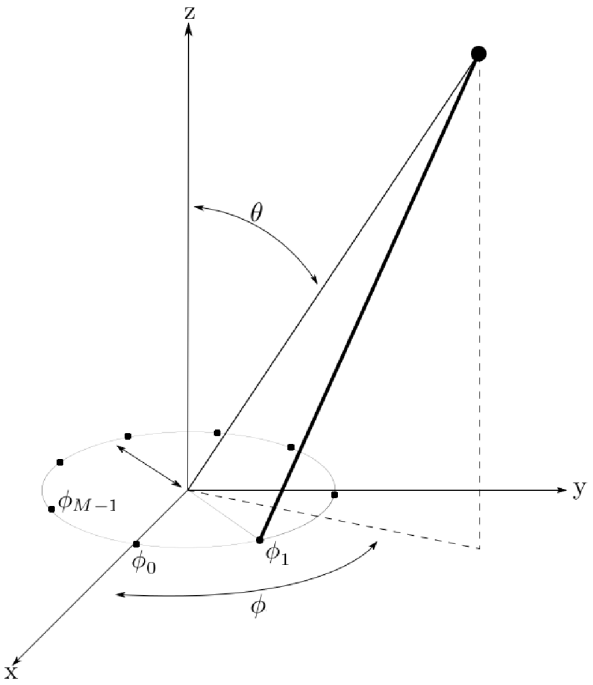

Figure 2-2: Circular geometry

states that all frequencies in the observed band B cause the same phase-shift when f_c is much higher than B. Therefore this spacing d in wavelengths holds true for all observed signals in that band, which simplifies the model of the array manifold, also referred to as the steering vector. This could lead to biased estimates of the angles if f_c is not much higher than B. When the frequency belonging to that angle is correctly estimated correction for this bias is possible.
Figure 2-2 depicts the circular array geometry. The dot on the x-axis represents the first value of the array manifold. The other dots represents the other antennas and θ represents the elevation, ϕ the azimuth and r the radius of the antenna array. The azimuth angle between the first antenna and the mth antenna is represented by ϕ_m and $\phi_m = \frac{2\pi m}{M}$. The array manifold this figure belongs to is represented by a column vector $\mathbf{a}_{uca}(\theta, \phi)$ [25]:

$$\mathbf{a}_{uca}(\theta,\phi) = \begin{bmatrix} a_1(\theta,\phi) \\ a_2(\theta,\phi) \\ \vdots \\ a_M(\theta,\phi) \end{bmatrix} = \begin{bmatrix} e^{jkr\sin(\theta)\cos(\phi)} \\ e^{jkr\sin(\theta)\cos(\phi-\frac{2\pi}{M})} \\ \vdots \\ e^{jkr\sin(\theta)\cos(\phi-\frac{2(M-1)\pi}{M})} \end{bmatrix} \tag{2-5}$$

Here θ and ϕ is the elevation and azimuth angle in radians, $k = \frac{2\pi}{\lambda}$, in which λ is the wavelength of the signal, is the wavenumber in radians per meter and r is the radius expressed in meters. To prevent ambiguities in the phase angle estimation, just like in a uniform linear array, the element spacing must be less than $\frac{\lambda}{2}$ [2].

Physical Effects of the Circular Geometry
The resolution of the elevation angles is at best when the signals arrive normal to the antenna array. This is because the result of $\sin\theta$, varies the most for small changes in θ when θ is close to 0 degrees. Noise will cause the estimates of the elevation to deviate around the true value, but when the resolution is poor this deviation will result in bigger errors than when the resolution is good. So the smaller the elevation angles the more accurate the elevation estimation is.

2-3 Complex Signal Representation

The frequency spectrum is divided in frequency bins and signals are modulated on a certain carrier frequency to transmit the original baseband signals. After the received signal passes a quadrature signal detector the carrier frequency, $f_{r,i}$, is down-converted to an intermediate frequency (IF) $f_{IF,i} = f_{r,i} - f_{lo}$. Here f_{lo} is the frequency of the local oscillator of the quadrature signal detector. From now on $f_{IF,i}$ is indicated by f_i and $s(t)$ represents the signal after they passed the quadrature detector. The ith down-converted signal, $s_i(t)$, is represented by the following formula [3]:

$$s_i(t) = \bar{s_i}(t)e^{j2\pi f_i t} \tag{2-6}$$

where $\bar{s_i}(t)$ is the complex envelope of the ith received signal and f_i is the intermediate frequency of the ith signal.

Every antenna receives the signal with a phase-shift determined by the array manifold and every signal has is multiplied with a complex scalar β. $\beta_i = b_i e^{-j2\pi\upsilon_i}$, in which the attenuation b_i and phase shift υ_i is caused by factors as the propagation distance and source power. The ith signal that is received on the mth antenna is described by the following equation:

$$x_m(t) = a_m \beta_i s_i(t) \tag{2-7}$$

The received signals are sampled with sample rate f_s, which must be at least twice the (maximum) intermediate frequency according to Nyquist Sampling Theorem [26] in order to estimate frequencies up to the intermediate frequency.

$$x_m[n] = x_m(nT_s) = x_m\Big(\frac{n}{f_s}\Big) \text{ with } n = 0, 1, \ldots, N-1 \tag{2-8}$$

Noise at the antenna elements is modeled by adding complex white Gaussian noise to the received signals.

The received signals are represented by a down-converted signal $s[n]$, an array manifold vector $\mathbf{a}_{uca}$ and a complex scalar β representing the amplitude and phase of the received signal. A

data matrix X, which is used in the algorithms, can be constructed by collecting the samples on each antenna element in a different row.

$$X = A_{uca}BS + W \tag{2-9}$$

with

$$A_{uca} = \left[\mathbf{a}_{uca}(\theta_1, \phi_1)\ \mathbf{a}_{uca}(\theta_2, \phi_2)\ \dots\ \mathbf{a}_{uca}(\theta_d\phi_d)\right] \in \mathbb{C}^{M,d} \tag{2-10}$$

$$B = \begin{bmatrix} \beta_1 & & & \emptyset \\ & \beta_2 & & \\ & & \ddots & \\ \emptyset & & & \beta_d \end{bmatrix} \in \mathbb{C}^{d,d} \tag{2-11}$$

$$S = \begin{bmatrix} s_1[0] & s_1[1] & \dots & s_1[N-1] \\ s_2[0] & s_2[1] & \dots & s_2[N-1] \\ \vdots & \vdots & \ddots & \vdots \\ s_d[0] & s_d[1] & \dots & s_d[N-1] \end{bmatrix} \in \mathbb{C}^{d,N} \tag{2-12}$$

$$W = \begin{bmatrix} w_1[0] & w_1[2] & \dots & w_1[N-1] \\ w_2[0] & w_2[2] & \dots & w_2[N-1] \\ \vdots & \vdots & \ddots & \vdots \\ w_M[0] & w_M[2] & \dots & w_M[N-1] \end{bmatrix} \in \mathbb{C}^{M,N} \tag{2-13}$$

$$\tag{2-14}$$

where d is the number of sources, M is the number of antennas and N is the number of samples. The array manifold $\mathbf{a}_{uca}(\theta_i, \phi_i)$ describes the phase shifts between the antenna elements that are caused by the ith source. This depends on the geometry of the antenna array and the direction from which the signal impinges the array. The direction of the ith source is defined by the azimuth ϕ_i and the elevation θ_i. $\beta_i = b_i e^{-j2\pi\upsilon_i}$ is a complex scalar in which the attenuation b_i and phase shift υ_i due to the propagation and source is taken into account. The complex white Gaussian noise of the nth sample for the mth antenna element is represented by $w_m[n]$. These noise samples of each element are collected in the noise matrix W.

Chapter 3

Transformation of Array Manifold

In a uniform linear array incoming plane waves arrive with a certain constant time delay between the antenna elements. In case of narrowband signals this results in the Vandermonde structure [27]. Unfortunately the uniform circular array is not of this form. A way to restore this form is with the theory of phase-mode excitation, which is described in Appendix B. The most important steps of the transformation are described in section 3-1.

3-1 Transformation to Beamspace

To understand the beamspace transformation it is important to understand that each element m of the array manifold of a UCA can be expressed as a sum of Bessel-functions [28]:

$$a_{\mathrm{UCA,m}}(\theta,\phi) = e^{jkr\sin(\theta)\cos(\phi-2\pi\frac{m}{M})} \tag{3-1}$$

$$= \sum_{q=-\infty}^{\infty} j^q J_q(kr\sin(\theta))e^{jq(\phi-2\pi\frac{m}{M})} \text{ for } m=0,1,\ldots,M-1 \tag{3-2}$$

where $a_{\mathrm{UCA,m}}(\theta,\phi)$ represents the mth entry of the uniform circular array manifold, which is described by a sum of Bessel-functions from $q=-\infty\, to\, \infty$. $J_q(kr\sin(\theta))$ represents the Bessel-function of the qth order with $kr\sin(\theta)$ as argument. Then a discrete Fourier Transform is performed over the array manifold. This results in the following Fourier Coefficients:

$$a_p(\theta,\phi) = \frac{1}{M}\sum_{m=0}^{M-1} a_{\mathrm{UCA,m}}(\theta,\phi)e^{j2\pi\frac{m}{M}p} \tag{3-3}$$

$$= \frac{1}{M}\sum_{m=0}^{M-1}\sum_{q=-\infty}^{\infty} j^q J_q(kr\sin(\theta))e^{jq(\phi-2\pi\frac{m}{M})}e^{j2\pi\frac{m}{M}p} \tag{3-4}$$

$$= \frac{1}{M}\sum_{q=-\infty}^{\infty} j^q J_q(kr\sin(\theta))e^{jq\phi}\sum_{m=0}^{M-1} e^{j2\pi\frac{m}{M}(p-q)} \tag{3-5}$$

where p is the phase-mode number. The last sum equals M in case the difference between p and q is M times an integer; $q-p=Ml$ where l is an integer. Otherwise it is zero, because the complex numbers over the unity circle cancel each other out. Therefore instead of the sum over all values of q the sum of l integers from $-\infty$ to ∞, where q is replaced by $p+Ml$, is used to represent this equation. This leads to the following equation:

$$a_p(\theta,\phi) = \sum_{l=-\infty}^{\infty} j^{p+Ml}J_{p+Ml}(kr\sin(\theta))e^{j(p+Ml)\phi} \text{ for } p=-\infty,\ldots,\infty \tag{3-6}$$

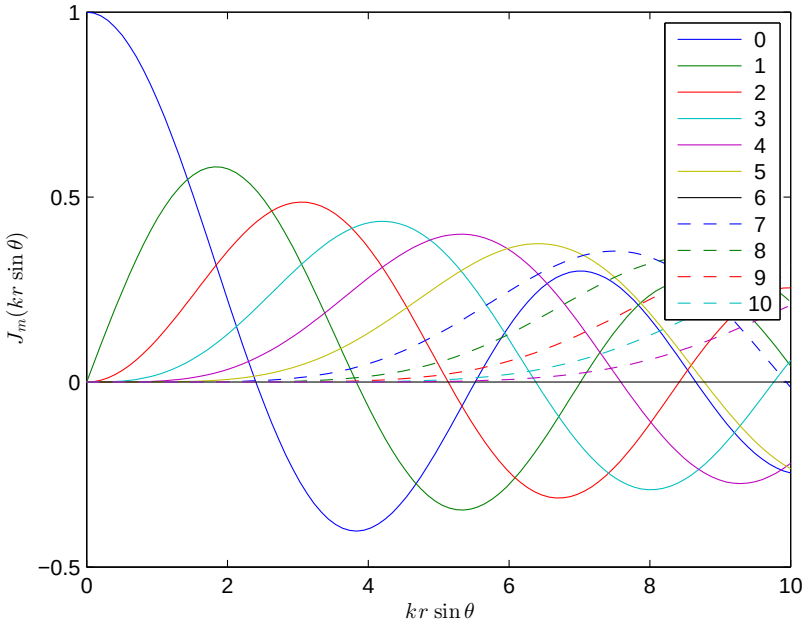

Figure 3-1: Behaviour of the Bessel Functions for varying orders (order is given in the legend) and arguments

When the order of the Bessel-function becomes larger than the argument, the result is more or less zero [2]. This is illustrated in figure 3-1 where each line represents the Bessel-function

of the order indicated by the legend. The goal now is to choose the number of phase-modes p and antennas M in a way that only when $l = 0$ the Bessel-function within the summation $a_p(\theta, \phi)$ is not approximately zero. This happens when p is small and M is big. Hyberg gives the following equation to compute the number of the maximum phase-mode P that cannot be neglected [28].

$$P = \lfloor kr \rfloor = \lfloor \frac{2\pi r}{\lambda} \rfloor \tag{3-7}$$

When the spacing between the antenna elements is fixed the radius r increases as the number of elements M increases. If M and P are well chosen equation 3-6 can be simplified to the following equation:

$$a_p(\theta, \phi) \approx j^p J_p(kr \sin(\theta)) e^{jp\phi} \tag{3-8}$$

and after multiplying each pth element by j^{-p} the resulting virtual uniform circular array manifold $\mathbf{a}_o(\theta, \phi)$ is as follows:

$$\mathbf{a}_o(\theta, \phi) = C_o \begin{bmatrix} j^{-P} J_{-P}(kr \sin(\theta)) e^{-jP\phi} \\ \vdots \\ j^0 (kr \sin(\theta)) \\ \vdots \\ j^P J_P(kr \sin(\theta)) e^{jP\phi} \end{bmatrix} = \begin{bmatrix} J_{-P}(kr \sin(\theta)) e^{-jP\phi} \\ \vdots \\ J_0(kr \sin(\theta)) \\ \vdots \\ J_P(kr \sin(\theta)) e^{jP\phi} \end{bmatrix} \tag{3-9}$$

where

$$C_0 = \begin{bmatrix} j^{-P} & & & & \\ & \ddots & & & \\ & & J_0 & & \\ & & & \ddots & \\ & & & & j^P \end{bmatrix} \tag{3-10}$$

The number of virtual elements $M_p = 2P + 1$, which is always an odd number. The phases of the elements in this virtual array are defined by the azimuth ot the signals and the magnitudes are dependent on the elevation. When the elevation θ is the same for all signals and known, the Vandermonde form can be obtained by multiplying the approximation with J_ζ [29]:

$$J_\zeta = \begin{bmatrix} \frac{1}{J_{-P}(kr \sin(\theta))} & & & & \\ & \ddots & & & \\ & & \frac{1}{J_0(kr \sin(\theta))} & & \\ & & & \ddots & \\ & & & & \frac{1}{J_P(kr \sin(\theta))} \end{bmatrix} \tag{3-11}$$

where $\zeta = kr\sin(\theta)$.

This leads to the following formula for the virtual ULA $\mathbf{a}_\zeta(\phi)$:

$$\mathbf{a}_\zeta(\phi) = J_\zeta \mathbf{a}_o(\theta,\phi) = \begin{bmatrix} e^{-jP\phi} \\ \vdots \\ 1 \\ \vdots \\ e^{jP\phi} \end{bmatrix} \tag{3-12}$$

3-2 Errors due to Finite Number of Elements

The phase-mode excitation transform is based on a perfect circle and a circular antenna array only approaches a circle. A bias in the azimuth estimation is caused since the array is not a perfect circular due to the finite number of elements [30]. Especially when the number of elements is small a circle is not approached very well, so errors occur. This errors appear as higher-order terms in equation 3-6. These higher-order terms have a magnitude that is defined by the Bessel-function. The higher the order of this Bessel-function the smaller the magnitude. The magnitude is also small when the argument, $kr\sin\theta$, of the Bessel-function is small. So for a fixed kr the error is the highest when the elevation $\theta = 90$. Belloni and Koivunen describe a method to reduce this error [30]. Since the error depends on the DOA it has to estimate the DOA first.
When applying a DOA estimation algorithm as ESPRIT or root-MUSIC the performance seems te be much better when an odd number of elements is used than when an even number of elements is used [30]. This can also be seen in figure 5-1 for an algorithm based on ESPRIT.
In equation 3-6 the terms where $l \geq 1$ are ignored in the model, but these terms give an systematic error in some cases. Especially the first order error, where $l = 1$ or $l = -1$, has a big contribution to the error as can be seen in table 1 in [30]. In [30] also an expression for the first order error, $\varepsilon^{(1)}$, which is represented in 3-13. This error consists of two parts: $\varepsilon^{(1)} = \varepsilon_1^{(1)} + \varepsilon_2^{(1)}$. In this error $\varepsilon_1^{(1)}$ is the error caused by the $l = 1$ term and $\varepsilon_2^{(1)}$ is the term caused by the $l = -1$ term.

$$\varepsilon_1^{(1)} = \begin{bmatrix} j^{(M+P)}J_{(M+P)}(\zeta)e^{-j(M+P)\phi} \\ j^{(M+P-1)}J_{(M+P-1)}(\zeta)e^{-j(M+P-1)\phi} \\ \vdots \\ j^{M}J_{M}(\zeta)e^{-jM\phi} \\ \vdots \\ j^{(M-P+1)}J_{(M-P+1)}(\zeta)e^{-j(M-P+1)\phi} \\ j^{(M-P)}J_{(M-P)}(\zeta)e^{-j(M-P)\phi} \end{bmatrix} \tag{3-13}$$

$$\varepsilon_2^{(1)} = \begin{bmatrix} j^{(M-P)}J_{(M-P)}(\zeta)e^{j(M-P)\phi} \\ j^{(M-P+1)}J_{(M-P+1)}(\zeta)e^{j(M-P+1)\phi} \\ \vdots \\ j^{M}J_{M}(\zeta)e^{jM\phi} \\ \vdots \\ j^{(M+P-1)}J_{(M+P-1)}(\zeta)e^{j(M+M-1)\phi} \\ j^{(M+P)}J_{(M+P)}(\zeta)e^{j(M+P)\phi} \end{bmatrix} \tag{3-14}$$

Except for the exponential part $\varepsilon_2^{(1)}$ is a flipped version of $\varepsilon_1^{(1)}$. The exponential parts are flipped conjugated versions of each other. In figure 3-1 it can be seen that for small ζ the Bessel-functions of small orders have a much bigger amplitude than bessel-functions of higher orders. The effect of this characteristic is that in the first-order error the terms where the order of the Bessel-function is small have the largest influence on the error. Especially the parts where $J_{(M-P)}(\zeta)$ have a big contribution. The lower part of $\varepsilon_1^{(1)}$ and the upper part of $\varepsilon_2^{(1)}$ have a small order Bessel-function and only those parts are therefore taken into account in the following equations, although the same principles described in the part below hold true for these ignored parts. The two vectors are combined by summing them and ignoring the upper part and the center of $\varepsilon_1^{(1)}$ and ignoring the lower part and center of $\varepsilon_2^{(1)}$. When the array manifold is transformed to the Vandermonde form the error is multiplied by C_o and J_ζ. Then the error looks as follows:

$$\mathbf{b}_\zeta(\phi) = J_\zeta \mathbf{a}_o(\phi) + J_\zeta C_o \varepsilon^{(1)} = \mathbf{a}_\zeta(\phi) + J_\zeta C_o \varepsilon^{(1)} \tag{3-15}$$

$$= \begin{bmatrix} e^{-jP\phi} \\ e^{-j(P-1)} \\ \vdots \\ 1 \\ \vdots \\ e^{j(P-1)} \\ e^{jP\phi} \end{bmatrix} + \begin{bmatrix} j^{(M-2P)}\frac{J_{(M-P)}(\zeta)}{J_P(\zeta)}e^{j(M-P)\phi} \\ j^{(M-2P+2)}\frac{J_{(M-P+1)}(\zeta)}{J_{P-1}(\zeta)}e^{j(M-P+1)\phi} \\ \vdots \\ \dots \\ \vdots \\ j^{M}\frac{J_{(M-P+1)}(\zeta)}{J_{-P+1}(\zeta)}e^{-j(M-P+1)\phi} \\ j^{M}\frac{J_{(M-P)}(\zeta)}{J_{-P}(\zeta)}e^{-j(M-P)\phi} \end{bmatrix} \tag{3-16}$$

The following equations are now useful:

$$J_p(\zeta) = (-1)^p J_p(\zeta) \tag{3-17}$$
$$j^{M-2p} = j^M j^{-2p} = j^M (-1)^{-p} \tag{3-18}$$

These equations can be used to transform 3-15:

$$\mathbf{b}_\zeta(\phi) = J_\zeta \mathbf{a}_o + J_\zeta C_o \varepsilon^{(1)} = \mathbf{a}_\zeta(\phi) + J_\zeta C_o \varepsilon^{(1)} \tag{3-19}$$

$$= \begin{bmatrix} e^{-jP\phi} \\ e^{-j(P-1)} \\ \vdots \\ 1 \\ \vdots \\ e^{j(P-1)} \\ e^{jP\phi} \end{bmatrix} + \begin{bmatrix} (-1)^{-P} j^M \frac{J_{(M-P)}(\zeta)}{J_P(\zeta)} e^{j(M-P)\phi} \\ (-1)^{-P+1} j^M \frac{J_{(M-P+1)}(\zeta)}{J_{P-1}(\zeta)} e^{j(M-P+1)\phi} \\ \vdots \\ \cdots \\ \vdots \\ (-1)^{P-1} j^M \frac{J_{(M-P+1)}(\zeta)}{J_{P-1}(\zeta)} e^{-j(M-P+1)\phi} \\ (-1)^{P} j^M \frac{J_{(M-P)}(\zeta)}{J_P(\zeta)} e^{-j(M-P)\phi} \end{bmatrix} \tag{3-20}$$

$$= \begin{bmatrix} e^{-jP\phi}[1 + (-1)^{-P} j^M \frac{J_{(M-P)}(\zeta)}{J_P(\zeta)} e^{jM\phi}] \\ e^{-j(P-1)\phi}[1 + (-1)^{-P+1} j^M \frac{J_{(M-P+1)}(\zeta)}{J_{P-1}(\zeta)} e^{jM\phi}] \\ \vdots \\ \cdots \\ \vdots \\ e^{j(P-1)\phi}[1 + (-1)^{P-1} j^M \frac{J_{(M-P+1)}(\zeta)}{J_{P-1}(\zeta)} e^{-jM\phi}] \\ e^{jP\phi}[1 + (-1)^{P} j^M \frac{J_{(M-P)}(\zeta)}{J_P(\zeta)} e^{-jM\phi} \end{bmatrix} \tag{3-21}$$

When ULA-ESPRIT is used the estimate ϕ the upper and lower $M_p - 1$ elements of the $\mathbf{a}_\zeta$ are selected.

$$\mathbf{a}_{a,\zeta}(\theta) = \triangle_{a,\theta} \mathbf{a}_\zeta(\theta) \tag{3-22}$$
$$\mathbf{a}_{b,\zeta}(\theta) = \triangle_{b,\theta} \mathbf{a}_\zeta(\theta) \tag{3-23}$$

where

$$\triangle_{a,\theta} = [I_{M_p-1}\ 0_1] \tag{3-24}$$
$$\triangle_{b,\theta} = [0_1\ I_{M_p-1}] \tag{3-25}$$

Then the Moore-Penrose pseudo-inverse, indicated by †, is used to obtain $e^{j\phi}$:

$$e^{j\phi} = \mathbf{a}^{\dagger}_{b,\zeta}(\theta)\mathbf{a}_{a,\zeta}(\theta) \tag{3-26}$$
$$= (\mathbf{a}^{H}_{b,\zeta}\mathbf{a}_{b,\zeta})^{-1}\mathbf{a}^{H}_{b,\zeta}\mathbf{a}_{a,\zeta}(\theta) \tag{3-27}$$

Since $(\mathbf{a}^{H}_{b,\zeta}\mathbf{a}_{b,\zeta})^{-1}$ is only a scalar and ϕ, the parameter of interest, is defined by the phase of the obtained result, this scalar can be ignored. So the equation becomes as follows:

$$\arg\{e^{j\phi}\} = \arg\{\mathbf{a}^{H}_{b,\zeta}\mathbf{a}_{a,\zeta}(\theta)\} \tag{3-28}$$

Then the complex conjugate of the pth element of $\mathbf{a}_{b,\zeta}$ is multiplied by the pth element of $\mathbf{a}_{a,\zeta}$:

$$\mathbf{a}^{H}_{b,\zeta}\mathbf{a}_{a,\zeta}(\theta) = \text{sum}\{a^{*}_{P,\zeta}a_{P-1,\zeta}(\theta) \ + \ a^{*}_{P-1,\zeta}a_{P-2,\zeta}(\theta) \ + \ \dots \ + \tag{3-29}$$
$$a^{*}_{-P+1,\zeta}a_{-P+2,\zeta}(\theta) \ + \ a^{*}_{-P,\zeta}a_{-P+1,\zeta}(\theta)\} \tag{3-30}$$

Each mth element in this $M_p - 1$-element sum has a counterpart at position $M_p - 1 - m$. In reality $\mathbf{b}_{\zeta}(\phi)$ instead of $\mathbf{a}_{\zeta}(\phi)$ is used and therefore an error is present in the terms in the sum. Then the errors in these counterparts cancel each other out in case an odd number of elements is used. This is shown by the following equations for the first and last elements in the sum, where $b_{p,\zeta}$ is the pth element of $\mathbf{b}_{\zeta}(\phi)$. For the following equation the Bessel-functions, which are real scalars, are interchanged:

$$Y = \frac{J_{(M-P+1)}(\zeta)}{J_P(\zeta)} \tag{3-31}$$
$$Z = \frac{J_{(M-P)}(\zeta)}{J_P(\zeta)} \tag{3-32}$$

This works as follows:

$$b^{*}_{P,\zeta}b_{P-1,\zeta}(\theta) \ + \ b^{*}_{-P+1,\zeta}b_{-P,\zeta}(\theta) \tag{3-33}$$
$$= \ [e^{-jP\phi}[1 + (-1)^{-P}j^{M}Ze^{jM\phi}]]^{*}[e^{-j(P-1)\phi}[1 + (-1)^{-P+1}j^{M}Ye^{jM\phi}]] \ + \tag{3-34}$$
$$[e^{j(P-1)\phi}[1 + (-1)^{P-1}j^{M}Ye^{-jM\phi}]]^{*}[e^{jP\phi}[1 + (-1)^{P}j^{M}Ze^{-jM\phi}] \tag{3-35}$$

The following equations are used to simplify equation 3-33:

$$(uv)^* = v^* u^* \tag{3-36}$$
$$(1+u)^* = (1+u^*) \tag{3-37}$$
$$(j^M)^* = (-j)^M \tag{3-38}$$

The order of the variables does not matter in case the variables are just values instead of vectors. So equation 3-33 can be rewritten to:

$$\begin{aligned} & b^*_{P,\zeta} b_{P-1,\zeta}(\theta) \ + \ b^*_{-P+1,\zeta} b_{-P,\zeta}(\theta) \\ = \ & [e^{jP\phi}[1+(-1)^{-P}(-j)^M Z e^{-jM\phi}]] \ [e^{-j(P-1)\phi}[1+(-1)^{-P+1} j^M Y e^{jM\phi}]] \ + \\ & [e^{-j(P-1)\phi}[1+(-1)^{P-1}(-j)^M Y e^{jM\phi}]] \ [e^{jP\phi}[1+(-1)^{P} j^M Z e^{-jM\phi}] \\ = \ & e^{i\phi}[[1+(-1)^{-P}(-j)^M Z e^{-jM\phi}][1+(-1)^{-P+1} j^M Y e^{jM\phi}] \ + \\ & [1+(-1)^{P-1}(-j)^M Y e^{jM\phi}][1+(-1)^{P} j^M Z e^{-jM\phi}]] \end{aligned} \tag{3-39}$$

When the term after $e^{j\phi}$ is just a scalar or in other words when it has no phase, there will be no bias.

$$[[1+(-1)^{-P}(-j)^M Z e^{-jM\phi}][1+(-1)^{-P+1} j^M Y e^{jM\phi}] \ + \\ [1+(-1)^{P-1}(-j)^M Y e^{jM\phi}][1+(-1)^{P} j^M Z e^{-jM\phi}] \tag{3-40}$$

$$= \ [[1+(-1)^{-P}(-j)^M Z e^{-jM\phi} + (-1)^{-P+1} j^M Y e^{jM\phi} + (-1)^{-2P+1} YZ] \ + \\ [1+(-1)^{P-1}(-j)^M Y e^{jM\phi} + (-1)^{P} j^M Z e^{-jM\phi} + (-1)^{-2P-1} YZ] \tag{3-41}$$

$$\tag{3-42}$$

This equation is a scaler when the phase-terms cancel each other out:

$$(-1)^{-P}(-j)^M Z e^{-jM\phi} + (-1)^P j^M Z e^{-jM\phi} = 0 \tag{3-43}$$
$$j^M + (-j)^M = 0 \tag{3-44}$$
$$(-1)^M (j)^M + j^M = 0 \tag{3-45}$$

and

$$(-1)^{-P+1} j^M Y e^{jM\phi} + (-1)^{P-1}(-j)^M Y e^{jM\phi} = 0 \tag{3-46}$$
$$j^M + (-j)^M = 0 \tag{3-47}$$
$$(-1)^M (j)^M + j^M = 0 \tag{3-48}$$

So if $(-1)^M = -1$ the terms cancel each other out. This happens if and only if M is odd. Therefore the error will be much bigger if the number of antenna elements is even then if it is odd.

Effect of the Elevation on the Estimation Performance
The transformation of the UCA manifold to a ULA manifold is a transformation of the geometry and has effect on the estimation performance for different angles. If the argument of the Bessel-function is small, the non-zero terms of the Bessel-functions in formula 3-6 are smaller, so it is more appropriate the discard them. So the estimation of the elevation and azimuth should be less biased if θ is close to zero, which is the case at angles that are perpendicular to the plane.

Chapter 4

ESPRIT-Based JAFE

The Estimation of Signal Parameters via Rotational Invariance Techniques (ESPRIT) algorithm gives numerical estimates from data that have a shift invariant structure. It attempts to separate the d signals from the noise by applying a singular value decomposition (SVD), which works in case the data matrix has a column rank d and $M-1 \geq d$, where M is the number of antenna elements. This results in a shift invariant signal subspace. This shift invariance makes it possible to estimate the parameters.

This chapter first describes JAFE for uniform linear arrays. The ESPRIT algorithm for 1-D DOA estimation with a UCA is described in section 4-2. Then it describes the ESPRIT algorithm for 2-D DOA estimation in section 4-3, which a simple version of the UCA-JAFE algorithm of Tuo Fu, Shi Jin, and Xiqi Gao [16]. This is followed by the extension of the algorithm to a JAFE algorithm for circular arrays in 4-4.

4-1 ULA JAFE

The array manifold matrix of an ULA for d signals is described by the following equation:

$$A = \begin{bmatrix} \mathbf{a}(\theta_1) & \mathbf{a}(\theta_2) & \dots & \mathbf{a}(\theta_d) \end{bmatrix} \tag{4-1}$$

$$= \begin{bmatrix} 1 & 1 & \dots & 1 \\ e^{i2\pi\triangle 1 \sin\theta_1} & e^{i2\pi\triangle 1 \sin\theta_2} & \dots & e^{i2\pi\triangle 1 \sin\theta_d} \\ \vdots & \vdots & \ddots & \vdots \\ e^{i2\pi\triangle M-1 \sin\theta_1} & e^{i2\pi\triangle M-1 \sin\theta_2} & \dots & e^{i2\pi\triangle M-1 \sin\theta_d} \end{bmatrix} \tag{4-2}$$

where θ is the direction of the signal in degrees, M is the number of antenna elements and $\triangle$ is the element spacing expressed in wavelengths of the signal. The shift-invariant structure of the ULA manifold vectors can be used the estimate the DOAs. In standard ULA-JAFE [3]

as described by A.N. Lemma first the data matrix X, as described in 2-9, is extended with temporal smoothing. This is done in order to obtain a shift-invariant structure in the columns from which the frequencies of signals can be estimated. With a temporal smoothing factor m this results in a matrix X_m which consists of m time-shifted versions of X stacked upon each other. To construct this matrix X_m consider the following vector $\mathbf{x}_k$, which represents a sample vector of the data matrix X:

$$\mathbf{x}_k = A\mathbf{s}[k] \in \mathbf{C}^{M,1} \tag{4-3}$$

$$\tag{4-4}$$

where A is consists of the ULA manifolds and the down-converted signals $\mathbf{s}[k]$. A signals $s[k]$ can be represented by $e^{j2\pi fk}\bar{s}[k]$. In this equation $\bar{s}$ is the baseband signal and f is the frequency of the signal. With this vector the temporal smoothed data matrix is formed as follows [3]:

$$X_m = \begin{bmatrix} \mathbf{x}_0 & \mathbf{x}_1 & \dots & \mathbf{x}_{N-m} \\ \mathbf{x}_1 & \mathbf{x}_2 & \dots & \mathbf{x}_{N-m+1} \\ \vdots & \vdots & \ddots & \vdots \\ \mathbf{x}_{m-1} & \mathbf{x}_m & \dots & \mathbf{x}_{N-1} \end{bmatrix} \tag{4-5}$$

$$= \begin{bmatrix} A\left[\bar{\mathbf{s}}[0] & \Omega\bar{\mathbf{s}}[1] & \dots & \Omega^{N-m}\bar{\mathbf{s}}[N-m]\right] & & \\ A\Omega\left[\bar{\mathbf{s}}[1] & \Omega\bar{\mathbf{s}}[2] & \dots & \Omega^{N-m}\bar{\mathbf{s}}[N-m+1]\right] & & \\ \vdots & & & & \vdots & \vdots \\ A\Omega^{m-1}\left[\bar{\mathbf{s}}[m-1] & \Omega\bar{\mathbf{s}}[m] & \dots & \Omega^{N-m}\bar{\mathbf{s}}[N-1]\right] & & \end{bmatrix} \tag{4-6}$$

where for d sources,

$$\bar{\mathbf{s}}[\mathbf{k}] = \begin{bmatrix} \bar{s}_1[k] \\ \bar{s}_2[k] \\ \vdots \\ \bar{s}_d[k] \end{bmatrix} \tag{4-7}$$

,

$$\Omega = \begin{bmatrix} \rho_1 & & & \\ & \rho_2 & & \\ & & \ddots & \\ & & & \rho_d \end{bmatrix} \tag{4-8}$$

and $\rho_i = e^{j2\pi f_i}$.

According to the narrowband assumption the following relation holds true for the baseband signals $\bar{s}(t)$:

$$\bar{\mathbf{s}}[n] \approx \bar{\mathbf{s}}[n+1] \approx \cdots \approx \bar{\mathbf{s}}[n+m] \tag{4-9}$$

Using this relation the stacked data matrix of 4-78 can be modeled as follows:

$$X_m = A_m F_s \tag{4-10}$$

where

$$A_m = \begin{bmatrix} A \\ A\Omega \\ \vdots \\ A\Omega^{m-1} \end{bmatrix} \tag{4-11}$$

and

$$F_s = [\mathbf{s}[0]\ \Omega\mathbf{s}[1]\ \ldots\ \Omega^{N-m}\mathbf{s}[N-m]] \tag{4-12}$$

The stacking causes a shift-invariant structure for Ω, ignoring A, when the signals are narrowband. This Ω contains the frequencies of the signals and must be estimated in order to compute the frequencies. The array manifolds of each signals are not directly available in practice, but are present in the signal subspace, which can be estimated with help of the singular value decomposition (SVD). The columns of the signal subspace $U_{m,s}$ have a shift invariant structure from which Ω can be estimated [3]. This works as follows. First the signal subspace of the extended data matrix Y_m is estimated:

$$X_m = U_m \Sigma_m V_m^H \tag{4-13}$$

$$= [U_{m,s}\ U_{m,n}] \begin{bmatrix} \Sigma_{m,s} & 0 \\ 0 & \Sigma_{m,n} \end{bmatrix} [V_{m,s}\ V_{m,n}]^H \tag{4-14}$$

The diagonal matrix Σ_m contains the singular values of the signals and the noise. If the signal-to-noise ratio is high enough and the matrix has rank d, the first d largest singular

values correspond to the singular values of the signal. From U_m the, $mM \times d$ sized, signal subspace $U_{m,s}$ can be extracted. Here M is the number of antenna elements.

$U_{m,s}$ is a mixture of the array manifold:

$$U_{m,s} = A_m T^{-1} \tag{4-15}$$

where T is an $d \times d$ transition matrix.

From A_m, m submatrices can be extracted which all contain A, see equation 4-11. To estimate the DOAs from A with ESPRIT, the upper $M-1$ and lower $M-1$ rows must be selected first. Since an extended matrix is used which consists of stacked versions of X and thus A, from all these stacked matrices the upper and lower $M-1$ rows can be used for the DOA estimation. An extended selection matrix can be used to extract m times $M-1$ upper and lower rows. This is done with I_m, an identity matrix of size m, and the kronecker product:

$$\triangle_{a,m,\theta} = I_m \otimes \triangle_{a,\theta} \tag{4-16}$$
$$\triangle_{b,m,\theta} = I_m \otimes \triangle_{b,\theta} \tag{4-17}$$

where

$$\triangle_{a,\theta} = [I_{M-1}\ 0_1] \tag{4-18}$$
$$\triangle_{b,\theta} = [0_1\ I_{M-1}] \tag{4-19}$$

Then $U_{a,\theta}$ and $U_{a,\theta}$ can be selected from $U_{s,m}$:

$$U_{a,\theta} = \triangle_{a,m,\theta} U_{m,s} \tag{4-20}$$
$$U_{b,\theta} = \triangle_{b,m,\theta} U_{m,s} \tag{4-21}$$

Although the left singular signal subspace is a mix of the array manifolds the following relationship holds true:

$$U_{a,\theta} = \triangle_{a,m,\theta} U_{m,s} = \triangle_{a,\theta} A_m T^{-1} \tag{4-22}$$
$$U_{b,\theta} = \triangle_{b,m,\theta} U_{m,s} = \triangle_{b,\theta} A_m T^{-1} = \triangle_{a,\theta} A_m \Theta_{ula} T^{-1} \tag{4-23}$$

where

$$\Theta_{ula} = \begin{bmatrix} e^{j2\pi\triangle \sin\theta_1} & & & \\ & e^{j2\pi\triangle \sin\theta_2} & & \\ & & \ddots & \\ & & & e^{j2\pi\triangle \sin\theta_d} \end{bmatrix} \tag{4-24}$$

Then:

$$U_{x,\theta}^{\dagger} U_{y,\theta} = T\theta T^{-1} \tag{4-25}$$

An eigenvalue decomposition on $U_{x,\theta}^{\dagger} U_{y,\theta}$ gives the eigenvalues on the diagonal of diagonal matrix Θ_{ula} and the eigenvectors in matrix T. Then the final step is to calculate the azimuth angles from the eigenvalues. The diagonal of Θ_{ula} contains d elements. The ith eigenvalue is described by $e^{j\theta_i}$, so the ith azimuth can be computed as follows:

$$\theta_i = \sin\{\frac{\arg(e^{j2\pi\triangle \sin\theta_i})}{2\pi\triangle}\} \tag{4-26}$$

To estimate the frequencies Ω must be estimated by from the extended array manifold 4-84. The first step is selecting the right submatrices $U_{a,\Omega}$ and $U_{b,\Omega}$ from $U_{m,s}$ as follows:

$$U_{a,\Omega} = \triangle_{a,M,\Omega} U_{m,s} \tag{4-27}$$
$$U_{b,\Omega} = \triangle_{b,M,\Omega} U_{m,s} \tag{4-28}$$

where the selection matrices $J_{a,\Omega}$ and $J_{b,\Omega}$ are formed in the following way:

$$\triangle_{a,M,\Omega} = [I_{m-1} \quad 0_1] \otimes I_M \tag{4-29}$$
$$\triangle_{b,M,\Omega} = [0_1 \quad I_{m-1}] \otimes I_M \tag{4-30}$$

The obtained matrices $U_{a,\Omega}$ and $U_{b,\Omega}$ can be expressed as follows:

$$U_{a,\Omega} = A_{a,\Omega} T^{-1} \tag{4-31}$$
$$U_{b,\Omega} = A_{b,\Omega} T^{-1} = A_{a,\Omega} \Omega T^{-1} \tag{4-32}$$

where $A_{a,\Omega}$ contains the first and $A_{b,\Omega}$ contains the last $(m-1)M$ rows of A_m and the transition matrix T here is the same as for the DOA estimation. This is what makes it possible to match the parameters with ESPRIT. Using the same matrix T for both DOA and frequency estimation from this temporal smoothed matrix is called joint diagonalization. The matching frequencies can be calculated from Ω and Ω can be obtained as follows [3]:

$$U_{a,\Omega}^{\dagger} U_{b,\Omega} = T A_{a,\Omega}^{\dagger} A_{a,\Omega} \Omega T^{-1} = T \Omega T^{-1} \tag{4-33}$$
$$\tag{4-34}$$

Since T is already obtained from the eigenvalue decomposition for DOA estimation it can be used here to calculate diagonal matrix Ω from $T\Omega T^{-1}$. Then the final step is to calculate the frequencies from the ith value on the diagonal of Ω:

$$f_i = \frac{\arg\rho}{2\pi} \tag{4-35}$$

4-2 Standard ESPRIT for 1-D DOA Estimation

In standard ESPRIT the SVD is performed on the ULA data matrix. When a UCA is used the data matrix X must be transformed to a virtual ULA matrix Y_o with the technique described in chapter 3. This is done by left multiplying the data with a Fourier transform matrix V^H which results in a matrix with N data samples on $M_p = 2P+1$ rows, which represent the phase modes [31]. This is multiplied with C_o, see 3-10.

$$Y_o = F_o^H X = C_o V^H X \ \in \ \mathbb{C}^{2P+1,N} \tag{4-36}$$

$$V^H = \ \sqrt{M}[w_{-P} \dots w_0 \dots w_P]^T \tag{4-37}$$
$$w_p^H = \ \tfrac{1}{M}[1 \ e^{j2\pi p/M} \dots e^{j2\pi pM/N}] \tag{4-38}$$

This transformation to Y_o is performed on X. The model of X is as follows: $X = A_{uca} BS$. The column vectors are described by the array manifold A_{uca}. This analysis focuses on A_{uca}, ignoring B and S

$$A_o = F_o^H A = C_o V^H A_{uca} \tag{4-39}$$

Then for d signals A_o looks as follows:

$$A_o = [\mathbf{a}_o(\theta_1, \phi_1) \ \mathbf{a}_o(\theta_2, \phi_2) \ \dots, \mathbf{a}_o(\theta_d, \phi_d)] \tag{4-40}$$

The columns of A_o contain the transformed array manifolds $\mathbf{a}_o(\theta, \phi)$, which contains $M_p = 2P + 1$ complex values:

$$\mathbf{a}(\theta, \phi)_o = \sqrt{M} \begin{bmatrix} J_{-P}(kr\sin(\theta))e^{-jP\phi} \\ \vdots \\ J_0(kr\sin(\theta)) \\ \vdots \\ J_P(kr\sin(\theta))e^{jP\phi} \end{bmatrix} \tag{4-41}$$

When the elevation θ is the same for each source and known, or some elevation angle is chosen, the Vandermonde form can be obtained by multiplying the approximation with J_ζ [29], where $\zeta = kr\sin(\theta)$, see equation 3-11. Then the multiplications performed on A_{uca} are as follows:

$$A_\zeta = J_\zeta F_o^H A = J_\zeta C_o V^H A_{uca} \tag{4-42}$$

where

$$A_\zeta = [\mathbf{a}_\zeta(\phi_1)\ \mathbf{a}_\zeta(\phi_2)\ \ldots, \mathbf{a}_\zeta(\phi_d)] \tag{4-43}$$

and

$$\mathbf{a}_\zeta(\phi) = \begin{bmatrix} e^{-jP\phi} \\ \vdots \\ 1 \\ \vdots \\ e^{jP\phi} \end{bmatrix} \tag{4-44}$$

Then the model of Y is as follows:

$$Y = A_\zeta B S \tag{4-45}$$

After complex white Gaussian noise is added to X in the simulation it is transformed too. Then a singular value decomposition on Y is performed, the signal and noise subspace, U_s and U_n respectively, are obtained:

$$Y = U\Sigma V^H \tag{4-46}$$

$$= [U_s\ U_n] \begin{bmatrix} \Sigma_s & 0 \\ 0 & \Sigma_n \end{bmatrix} [V_s\ V_n]^H \tag{4-47}$$

The diagonal matrix Σ contains the singular values of the signals and the noise sorted by the magnitudes in descending order. If the signal-to-noise ratio is high enough and the matrix is not rank deficient the first d largest singular values correspond to the singular values of the signal. From U the signal subspace $M \times d$ sized U_s can be extracted, which contains the signal direction vectors.

U_s is a mixture of the array manifolds:

$$U_s = A_\zeta T^{-1} \tag{4-48}$$

where T is an $d \times d$ transition matrix, which describes how the estimated array manifolds are mixed.

Then with selection matrices $\triangle_{a,\Phi}$ and $\triangle_{b,\Phi}$ two submatrices are selected form the signal subspace:

$$U_{x,\Phi} = \triangle_{a,\Phi} U_s \tag{4-49}$$
$$U_{y,\Phi} = \triangle_{b,\Phi} U_s \tag{4-50}$$

where

$$\triangle_{a,\Phi} = [I_{M-1}\ 0_1] \tag{4-51}$$
$$\triangle_{b,\Phi} = [0_1\ I_{M-1}] \tag{4-52}$$

Due to the shift invariance in A_ζ the obtained matrices $U_{a,\Phi}$ and $U_{b,\Phi}$ can be expressed as follows [3]:

$$U_{a,\Phi} = \triangle_{a,\Phi} U_s = \triangle_{a,\Phi} A_\zeta T^{-1} \tag{4-53}$$
$$U_{b,\Phi} = \triangle_{b,\Phi} U_s = \triangle_{b,\Phi} A_\zeta T^{-1} = \triangle_{a,\Phi} A_\zeta \Phi T^{-1} \tag{4-54}$$

where

$$\Phi = \begin{bmatrix} e^{j\phi_1} & & & \\ & e^{j\phi_2} & & \\ & & \ddots & \\ & & & e^{j\phi_d} \end{bmatrix} \tag{4-55}$$

Then:

$$U_{x,\Phi}^{\dagger} U_{y,\Phi} = T\Phi T^{-1} \tag{4-56}$$

An eigenvalue decomposition on $U_{x,\Phi}^{\dagger} U_{y,\Phi}$ gives the eigenvalues in matrix Φ and the eigenvectors in matrix T. Then the final step is to calculate the azimuth angles from the eigenvalues. The diagonal of Φ contains d elements. The ith element is described by $e^{j\phi_i}$, so the ith azimuth can be computed as follows:

$$\phi_i = \arg(e^{j\phi_i}) \tag{4-57}$$

4-3 2-D Direction of Arrival Estimation

This algorithm is a simple version of the UCA-JAFE algorithm of Tuo Fu, Shi Jin, and Xiqi Gao [16]. For 2-D DOA estimation the UCA manifold must be transformed according to equation 4-39 in order to obtain array manifolds of the form of equation 4-41.

After the beamspace transformation, the columns of A_o contain the virtual linear array manifold $\mathbf{a}_o(\theta, \phi)$ that consists of M_p elements. Each element p is described as follows [31]:

$$a_{o,p}(\theta, \phi) = \sqrt{M} J_p(kr\sin(\theta)) e^{jp\phi} \text{ for } -P < p < P \tag{4-58}$$

To find both the elevation and azimuth angles the following relationship of the Bessel function can be used [31]:

$$\frac{2p}{\zeta} J_p(\zeta) = J_{p-1}(\zeta) + J_{p+1}(\zeta) \tag{4-59}$$

When ζ is replaced by $kr\sin(\theta)$ this equation looks as follows:

$$\frac{2p}{krsin(\theta)} J_p(kr\sin(\theta)) = J_{p-1}(kr\sin(\theta)) + J_{p+1}(kr\sin(\theta)) \tag{4-60}$$

From the top to the bottom every element of $\mathbf{a}_o(\theta, \phi)$ represents the exited phase-mode p beginning at $-P$ and incremented by 1 until row P. So when three submatrices are formed by selected the upper, middle and lower $M_p - 2$ rows, these matrices have a similar relationship:

$$\Lambda \mathbf{a}(\theta, \phi)_{o,y} = \sin\theta e^{j\phi} \mathbf{a}(\theta, \phi)_{o,x} + \sin\theta e^{-j\phi} \mathbf{a}(\theta, \phi)_{o,z} \tag{4-61}$$

where

$$\Lambda = \frac{2}{kr}\begin{bmatrix} -P+1 & & & & & & \\ & -P+2 & & & & & \\ & & \ddots & & & & \\ & & & 0 & & & \\ & & & & \ddots & & \\ & & & & & P-2 & \\ & & & & & & P-1 \end{bmatrix} \tag{4-62}$$

,

For multiple signals A_x, A_y and A_z can be extracted from A, where A_x contains the upper $M_p - 2$ rows, A_y contains the middle $M_p - 2$ rows and A_z contains the lower $M_p - 2$ rows. Subsequently this equation can be rewritten to:

$$\Lambda A_y = \Upsilon A_x + \Upsilon^* A_z \tag{4-63}$$

$$= \begin{bmatrix} A_x & A_z \end{bmatrix} \times \begin{bmatrix} \Upsilon \\ \Upsilon^* \end{bmatrix} \tag{4-64}$$

where for d sources

$$\Upsilon = \begin{bmatrix} \psi_1 & & & \\ & \psi_2 & & \\ & & \ddots & \\ & & & \psi_d \end{bmatrix} \tag{4-65}$$

and $\psi_i = \sin\theta_i e^{j\phi_i}$. Of course the array manifold A_o is not available, but $U_s = A_o T^{-1}$ is available after the selection of the first d columns of the signal subspace that is the output of the singular value decomposition performed on Y_o. The relationship still holds true for the rows of U_s. So now the same selection of three matrices from A_o is done for U_s. The following multiplication must be done to select the right submatrices:

$$U_{s,x} = \triangle_x U_s \tag{4-66}$$

$$U_{s,y} = \triangle_y U_s \tag{4-67}$$

$$U_{s,z} = \triangle_z U_s \tag{4-68}$$

where the selection matrices $\triangle_x$, $\triangle_y$ and $\triangle_z$ are built as follows:

$$\triangle_x = [I_{Mp}\ 0_{Mpx1}\ 0_{Mpx1}] \tag{4-69}$$
$$\triangle_y = [0_{Mpx1}\ I_{Mp}\ 0_{Mpx1}] \tag{4-70}$$
$$\triangle_z = [0_{Mpx1}\ 0_{Mpx1}\ I_{Mp}] \tag{4-71}$$

Equation 4-64 can be transformed to estimate Υ. When the system is overdetermined unique solutions for ψ can be obtained. This happens when $M_p - 2 > 2d$ [32].

$$\begin{bmatrix} \Upsilon \\ \Upsilon^* \end{bmatrix} = [A_x\ A_z]^\dagger \Lambda A_y \tag{4-72}$$

where $\dagger$ is used to denote the Moore-Penrose pseudo-inverse. Since $U_s = A_\zeta T^{-1}$ the submatrices of the subspace have the same relationship with T: $U_{s,x} = A_x T^{-1}$, $U_{s,y} = A_y T^{-1}$ and $U_{s,z} = A_z T^{-1}$. Therefore the following equation can be used to estimate Υ with an eigenvalue decomposition [32]:

$$\begin{bmatrix} T\Upsilon T^{-1} \\ T\Upsilon^* T^{-1} \end{bmatrix} = [U_{s,x}\ U_{s,z}]^\dagger \Lambda U_{s,y} \tag{4-73}$$

By taking the eigenvalues of $T\Upsilon T^{-1}$, which is the upper half of the obtained matrix after the right-hand side multiplication, the azimuths and elevations can be obtained with the following formulas [31]:

$$\theta_i = \arcsin(|\psi_i|) \tag{4-74}$$
$$\phi_i = \arg(\psi_i) \tag{4-75}$$

This part of the algorithm can estimate the 2-D DOAs of up to $\lfloor \frac{M_p-2}{2} \rfloor$ uncorrelated signals [33].

4-4 Joint Angle-Frequency Estimation

Just as in JAFE for ULAs the data matrix Y used for DOA estimation has to be extended in order to estimate the frequencies. This is done in a similar way as for ULA-JAFE. Let $\mathbf{y}_k$ represent a sample vector of the data matrix:

$$\mathbf{y}_k = A\mathbf{s}[k] \in \mathbf{C}^{M,1} \tag{4-76}$$
$$\tag{4-77}$$

where A can be the transformed array manifold A_o or A_ζ and $\mathbf{s}$ contains the down-converted signals, which can be represented as $s_i[k] = \bar{s}[k]e^{i2\pi f_i k}$, where $\bar{s}[k]$ is the baseband signal and f_i is the frequency of the ith signal. Then the new data matrix is formed as follows:

$$Y_m = \begin{bmatrix} \mathbf{y}_0 & \mathbf{y}_1 & \cdots & \mathbf{y}_{N-m} \\ \mathbf{y}_1 & \mathbf{y}_2 & \cdots & \mathbf{y}_{N-m+1} \\ \vdots & \vdots & \ddots & \vdots \\ \mathbf{y}_{m-1} & \mathbf{y}_m & \cdots & \mathbf{y}_{N-1} \end{bmatrix} \tag{4-78}$$

$$= \begin{bmatrix} A\begin{bmatrix}\overline{\mathbf{s}}[0] & \Omega\overline{\mathbf{s}}[1] & \dots & \Omega^{N-m}\overline{\mathbf{s}}[N-m]\end{bmatrix} & & & \\ A\Omega\begin{bmatrix}\overline{\mathbf{s}}[1] & \Omega\overline{\mathbf{s}}[2] & \dots & \Omega^{N-m}\overline{\mathbf{s}}[N-m+1]\end{bmatrix} & & & \\ \vdots & & \vdots & \vdots \\ A\Omega^{m-1}\begin{bmatrix}\overline{\mathbf{s}}[m-1] & \Omega\overline{\mathbf{s}}[m] & \dots & \Omega^{N-m}\overline{\mathbf{s}}[N-1]\end{bmatrix} & & & \end{bmatrix} \tag{4-79}$$

where for d sources,

$$\Omega = \begin{bmatrix} \rho_1 & & & \\ & \rho_2 & & \\ & & \ddots & \\ & & & \rho_d \end{bmatrix} \tag{4-80}$$

where $\rho_i = e^{i2\pi f_i}$, and

$$\overline{\mathbf{s}}[\mathbf{k}] = \begin{bmatrix} \bar{s}_1[k] \\ \bar{s}_2[k] \\ \vdots \\ \bar{s}_d[k] \end{bmatrix} \tag{4-81}$$

According to the narrowband assumption the following relation holds true for the baseband signals $\bar{s}(t)$:

$$\overline{\mathbf{s}}[n] \approx \overline{\mathbf{s}}[n+1] \approx \cdots \approx \overline{\mathbf{s}}[n+m] \tag{4-82}$$

Using this relation the stacked data matrix of 4-78 becomes as follows:

$$Y_m = A_m F_s \tag{4-83}$$

where

$$A_m = \begin{bmatrix} A \\ A\Omega \\ \vdots \\ A\Omega^{m-1} \end{bmatrix} \tag{4-84}$$

and

$$F_s = [\mathbf{s}[0]\ \Omega\mathbf{s}[1]\ \ldots\ \Omega^{N-m}\mathbf{s}[N-m]] \tag{4-85}$$

The stacking causes a shift-invariant structure for Ω when the signals are narrowband. This Ω contains the frequencies of the signals and must be estimated. After the signal subspace is extracted with help of the singular value decomposition the columns of the signal subspace $U_{m,s}$ have a shift invariant structure from which Ω can be estimated [3]. The method used works as follows. First the signal subspace of the extended data matrix Y_m is estimated:

$$Y_m = U_m \Sigma_m V_m^H \tag{4-86}$$

$$= [U_{m,s}\ U_{m,n}] \begin{bmatrix} \Sigma_{m,s} & 0 \\ 0 & \Sigma_{m,n} \end{bmatrix} [V_{m,s}\ V_{m,n}]^H \tag{4-87}$$

The diagonal matrix Σ_m contains the singular values of the signals and the noise. If the signal-to-noise ratio is high enough and the matrix is not rank deficient, the first d largest singular values correspond to the singular values of the signal. From U_m the, $mM \times d$ sized, signal subspace $U_{m,s}$ can be extracted. Here M_p is the number of virtual antenna elements.

$U_{m,s}$ is a mixture of the array manifold:

$$U_{m,s} = A_m T^{-1} \tag{4-88}$$

where T is an $d \times d$ transition matrix.

From A_m, m submatrices can be extracted which all contain A, see equation 4-84. From the stacked submatrices the 1-D DOAs (only azimuth, fixed elevation) or 2-D DOAs (azimuth

and elevation) can be estimation as described in section 4-2 and 4-3, respectively, depending on whether A_ζ or A_o is used. To do this correctly the selection matrices for DOA estimation must be expanded. This is done with I_m, an identity matrix of size m, and the kronecker product:

$$\triangle_{a,m} = I_m \otimes \triangle_a \tag{4-89}$$
$$\triangle_{b,m} = I_m \otimes \triangle_b \tag{4-90}$$

and

$$\triangle_{x,m} = I_m \otimes \triangle_x \tag{4-91}$$
$$\triangle_{y,m} = I_m \otimes \triangle_y \tag{4-92}$$
$$\triangle_{z,m} = I_m \otimes \triangle_z \tag{4-93}$$

Then the DOA algorithms can be used in the same manner as before only with these extended selection matrices.
To estimate the frequencies Ω must be estimated by selecting the right submatrices $U_{a,\Omega}$ and $U_{b,\Omega}$ from $U_{m,s}$ as follows:

$$U_{a,\Omega} = \triangle_{a,\Omega} U_{m,s} \tag{4-94}$$
$$U_{b,\Omega} = \triangle_{b,\Omega} U_{m,s} \tag{4-95}$$

where the selection matrices $J_{a,\Omega}$ and $J_{b,\Omega}$ are formed in the following way:

$$\triangle_{a,\Omega} = [I_{m-1} \quad 0_1] \otimes I_{M_p} \tag{4-96}$$
$$\triangle_{b,\Omega} = [0_1 \quad I_{m-1}] \otimes I_{M_p} \tag{4-97}$$

The obtained matrices $U_{a,\Omega}$ and $U_{b,\Omega}$ can be expressed as follows:

$$U_{a,\Omega} = A_{a,\Omega} T^{-1} \tag{4-98}$$
$$U_{b,\Omega} = A_{b,\Omega} T^{-1} = A_{a,\Omega} \Omega T^{-1} \tag{4-99}$$

where $A_{a,\Omega}$ contains the first and $A_{b,\Omega}$ contains the last $(m-1)M_p$ rows of A_m and the transition matrix T here is the same as for the DOA estimation. This is what makes it possible

to match the parameters with ESPRIT. Using this matrix T for both DOA and frequency estimation from this temporal smoothed matrix is called joint diagonalization. The matching frequencies can be calculated from Ω and Ω can be obtained as follows [3]:

$$U_{a,\Omega}^{\dagger} U_{b,\Omega} = T A_{a,\Omega}^{\dagger} A_{a,\Omega} \Omega T^{-1} = T \Omega T^{-1} \tag{4-100}$$

$$\tag{4-101}$$

Since T is already obtained from the eigenvalue decomposition for DOA estimation it can be used here to calculate Ω. Then the final step is to calculate the frequencies from the ith value on the diagonal of Ω:

$$f_i = \frac{\arg\rho}{2\pi} \tag{4-102}$$

4-5 Summary of 1-D DOA and 2-D DOA algorithm

In this section a summary of both algorithms is given.

Algorithm 1: JAFE algorithm with 1-D DOA estimation

1: Construct a temporal smoothed matrix X_m with temporal smoothing factor $m \geq 1$.
2: Compute $P = \lfloor kr \rfloor$ and perform the beamspace transform and divide the elements by the inverse Bessel function coefficients: $Y_{m,\zeta} = (I_m \otimes J_\zeta C_o V^H) X_m$.
3: Perform SVD on data matrix $Y_{m,\zeta}$ and apply a detection algorithm to estimate the number of sources d. Then extract the d left singular vectors that belong to the highest d singular values and form the signal subspace $U_{m,s}$.
4: Use the right selection matrices: $U_{a,\Phi} = \triangle_{a,m} U_{m,s} \Phi$ and $U_{a,\Phi} = \triangle_{b,\Omega} U_{m,s}$.
5: Perform an eigenvalue decomposition on $U_{a,\Phi}^{\dagger} U_{b,\Phi}$ to obtain diagonal matrix Φ with the eigenvalues and transition matrix T with the eigenvectors.
6: Select $U_{a,\Omega} = ([I_{m-1} \quad 0_1] \otimes I_{M_p}) U_{m,s}$ and $U_{b,\Omega} = ([0_1 \quad I_{m-1}] \otimes I_{M_p}) U_{m,s}$. Then compute $T^{-1} U_{a,\Omega}^{\dagger} U_{b,\Omega} T = \Omega$ with matrix T obtained from the previous step.
7: Φ contains eigenvalues ϕ on its diagonal and Ω contains eigenvalues ρ on its diagonal. For the ith signals the azimuth $\phi_i = \arg(e^{j\phi_i})$ and the frequency $f_i = \frac{\arg\rho}{2\pi}$.

Algorithm 2: JAFE algorithm with 2-D DOA estimation

1: Construct a temporal smoothing matrixed matrix X_m with temporal smoothing factor $m \geq 1$.
2: Compute $P = \lfloor kr \rfloor$ and perform the beamspace transform: $Y_{m,o} = (I_m \otimes C_o V^H) X_m$.
3: Perform SVD on data matrix $Y_{m,o}$ and apply a detection algorithm to estimate the number of sources d. Then extract the d left singular vectors that belong to the highest d singular values and form the signal subspace $U_{m,s}$.
4: Use the selection matrices: $U_{s,x} = \triangle_{x,m} U_{s,m}$, $U_{s,y} = \triangle_{y,m} U_{s,m}$ and $U_{s,z} = \triangle_{z,m} U_{s,m}$.
5: Compute $\left[[T\Upsilon T^{-1}]^T \ [T\Upsilon T^{-1}]^H\right]^T = [U_{s,x} \ U_{s,z}]^\dagger \Lambda U_{s,y}$.
6: Perform an eigenvalue decomposition on $T\Upsilon T^{-1}$ to obtain diagonal matrix Υ with the eigenvalues and transition matrix T with the eigenvectors.
7: Select $U_{a,\Omega} = ([I_{m-1} \quad 0_1] \otimes I_{M_p}) U_{m,s}$ and $U_{b,\Omega} = ([0_1 \quad I_{m-1}] \otimes I_{M_p}) U_{m,s}$. Then compute $T^{-1} U_{a,\Omega}^\dagger U_{b,\Omega} T = \Omega$.
8: Υ contains eigenvalues ψ on its diagonal and Ω contains eigenvalues ρ on its diagonal. For the ith signals the azimuth $\phi_i = \arg(\psi_i)$, the elevation $\theta_i = \arcsin(|\psi_i|)$ and the frequency $f_i = \frac{\arg \rho}{2\pi}$.

Chapter 5

Evaluation of the JAFE-Algorithm

In this chapter the performance of the ESPRIT-based JAFE-algorithms is investigated for different scenarios. Section 5-1 describes the effect of the number of antenna elements on the estimation error. Then the relation between the SNR and the number of samples is investigated in section 5-2. This is followed by an investigation about the influence of the sample frequencies on the RMSE of the azimuth, elevation and frequency when number of samples is constant in section 5-3. The signals used in the simulations are constructed as described in appendix A.

5-1 Effects of the Array Geometry

In this section the effect of the array geometry on the performance of the 2-D JAFE-algorithm is investigated. In section 5-1-1 the effect of the number of elements on the systematic error in the azimuth estimation is investigated, because the accuracy of the approximations in the transformation of the UCA manifold to the virtual UCA manifold, A_o, is influenced by the number of elements, see equation 3-8. Section 5-1-2 shows how the algorithm performs in noisy environments for different numbers of antenna elements.

5-1-1 Noiseless Case

The beamspace transform requires that the number of elements is higher than the number of phase-modes. Otherwise systematic errors occur due to the improper approximations made in the transform by discarding the non-zero Bessel coefficients. Here the effect of the number of physical antenna elements on the correctness of the approximations is investigated. The systematic error is not exactly the same for every azimuth angle as can be seen in figure 6-1 for an antenna array of 5 elements. The peak is the worst-case root-mean-square error (RMSE) of the azimuth and the angle at which this peak occurs is dependent on the number of antenna elements. For the simulation this peak error for each number of antenna elements

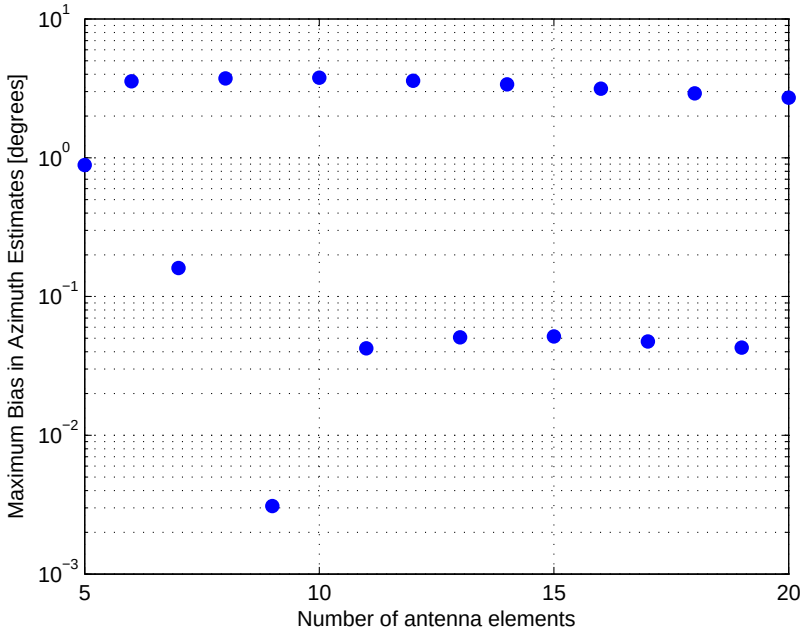

Figure 5-1: Performance in case of a varying number of elements

is chosen. In Figure 5-1 the maximum systematic azimuth error is given for a varying number of antenna elements from 5 to 20. The number of phase-modes is chosen according to formula 3-7 and the spacing between the antenna elements is $\frac{\lambda}{2}$. In this simulation $N = 100$, $\beta = 1$, $\theta = 90$ degrees, $\phi = 70$ degrees, $f = 100$ Hz, $f_s = 1$ kHz and the temporal smoothing factor $m = 10$. No spatial smoothing is used. Figure 5-1 shows that when the number of antenna elements is even the bias in the DOA estimation has larger peaks than when the number of antenna elements is odd. The reason for this is not that the error made in the transformation is bigger, but that for an odd number of elements the first-order error, which is the biggest part, has no influence. This first-order error is the error caused by neglecting the Bessel-function contributions for $l = 1$ in equation 3-6. In case of an odd number of elements the error in elements $-P$ to P of the vector cancel each other out as explained in section 3-2. For $5, 7, 9$ and 11 antenna elements the RMSE of the azimuth decreases when the number of elements increases. For higher number of elements the RMSE of the azimuth is more or less the same. Notice that the number of phase-modes that cannot be neglected increases when the radius r increases. This can be seen in formula 3-7 by looking at the radius r. In case of a fixed antenna elements spacing this happens as the number of antenna elements increases according. The Bessel-functions of a higher order represents higher phase-modes that are excited. As seen in figure 3-1 the magnitude of the Bessel-functions descends for increasing orders, but does not become zero. This is the same with the error when formula 3-7 is used.

5-1-2 Influence of Noise

In this section the effect of the number of antennas is investigated in presence of additional complex white Gaussian noise. When the antenna array has more elements, more spatial

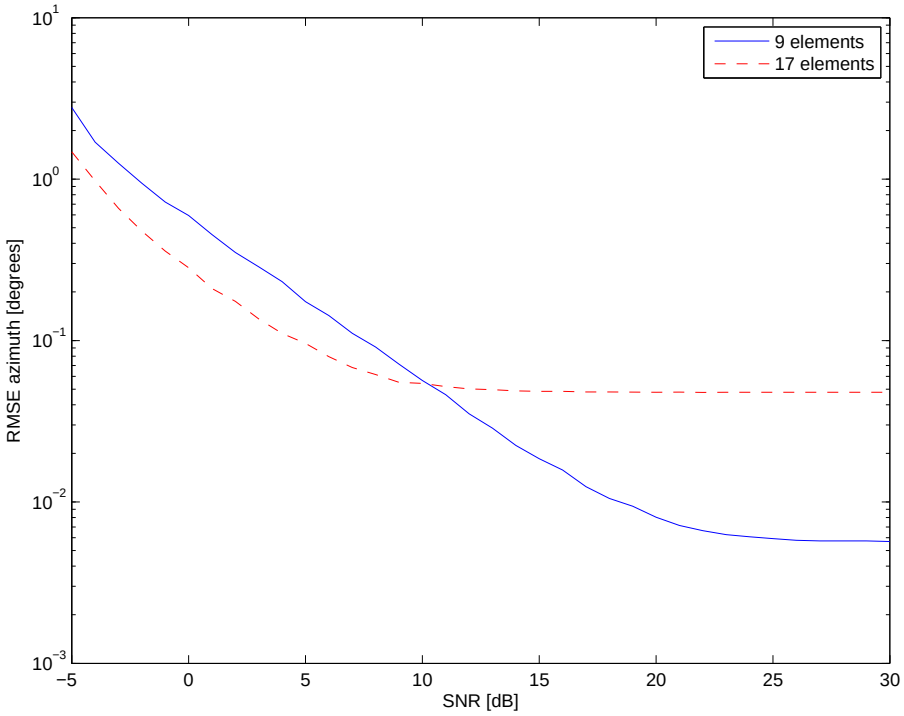

Figure 5-2: Effect of the signal-to-noise ratio on the PME azimuth estimation error for (a) 9 elements and (b) 17 elements

samples are taken at once at each sampling time. With more samples the variance of independent Gaussian variables decreases, which leads to more accurate estimates. For this simulation $N = 100$, $\beta = 1$, $\theta = 90$ degrees, $\phi = 70$ degrees, $f = 100$ Hz, $f_s = 1$ kHz and the temporal smoothing factor $m = 10$. No spatial smoothing is used and the element spacing is 0.42λ. Figure 5-2 shows that, while the systematic error of more elements than 9 may be lower, in noisy situations more antenna elements lead to lower RMSE than fewer antenna elements. When the same number of phase-modes is used for antennas with more elements instead of taking the maximum of equation 3-7, the systematic error may be lower, but too few phase-modes leads to systematic errors too and affects the resolution [34].

5-1-3 Conclusion

An odd number of elements seems to lead to a smaller RMSE in the azimuth estimation. For an odd number of elements the RMSE does not decrease significantly for when more than 11 elements are used. The systematic error is remarkably low with 9 antenna elements, but figure 5-2 shows that for low SNR the azimuth estimation with 17 elements is better. So depending on the noise an array of 9 elements can be better than an array of 17 elements. This simulation is performed for two antenna array with a fixed element spacing, so the aperture of the antenna array with 17 elements is bigger than that of the antenna array with 9 elements, which may causes the improved performance, but the fact that there are more spatial samples play a role too.

5-2 Effect of the Number of Samples and Different SNRs

In this section the effect of the number of samples on the performance of the algorithm is evaluated for different SNRs. For this investigation the 2-D DOA JAFE algorithm is used.

5-2-1 Spatial versus Temporal Samples

The data matrix is constructed from the sample data which are subject to noise. To reproduce the true version of these matrices theoretically an infinite number of samples are required, but depending on the SNR, a very proper approximation can be made with a finite number of samples.

The effect of the SNR and number of samples on the RMSE of the parameter estimation is investigated for 9 and 17 antenna elements. Figure 5-3 shows the effect for both situations. For these simulations one signal that impinges the array from $\theta = 50$ degrees and $\phi = 70$ degrees is used, $f = 200$ Hz, $f_S = 1$ kHz. the element spacing of $d = 0.42\lambda$, no spatial smoothing is used and the temporal smoothing factor $m = 10$.

5-2-2 Conclusion

At -15 dB both simulations result in an error of circa 103.9 degrees, because the singular value decomposition is not able to separate the signal subspace from the noise, and the RMS value of totally random estimates between -180 and 180 degrees is $\sqrt{\frac{1}{360}\int_{-180}^{180}\phi^2 d\phi} = 103.923$ degrees. It is clear that more antennas causes the algorithm to converge faster to the true azimuth angle when the number of samples or the SNR is increased. The simulation shows that when more antennas are used the required number of samples to achieve a certain RMSE is smaller. A reason for this is that more antennas lead to more spatial samples. Notice that the array of 17 elements has a bigger aperture too.

5-3 Effect of Different Sample Times with a Constant Number of Samples

In this section the effect of the sample rate on the RMSE is investigated for the 2-D DOA JAFE-algorithm. This should show if it is better to sample very fast over a part of a period, to sample a couple of periods or to sample slow so that the samples are distributed over a lot of periods. For the simulations a QPSK-signal is used as described in appendix A.

5-3-1 Dependency on Sample Time and Frequency

All samples have a signal component and a noise component. When infinite samples are taken these noise samples cancel each other out. In practice a finite sample set is obtained and the noise is not fully canceled out. The noise causes errors in the parameter estimation. For frequency estimation Nyquist stated that at least two samples per period are required for detection of that frequency. So a signal sequence of $\frac{N}{2}$ periods can be sampled with two

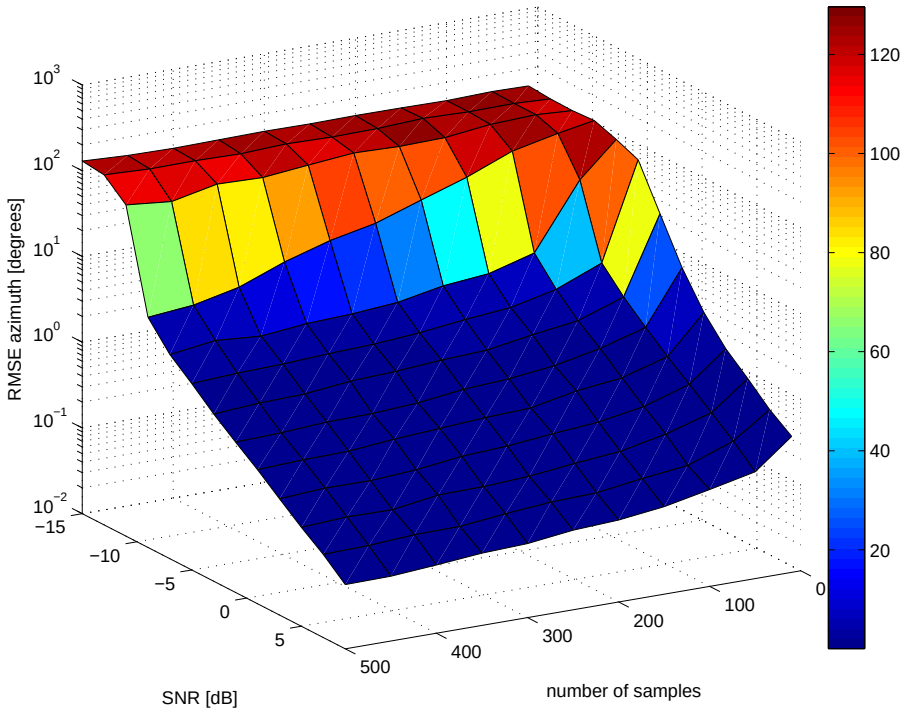

(a)

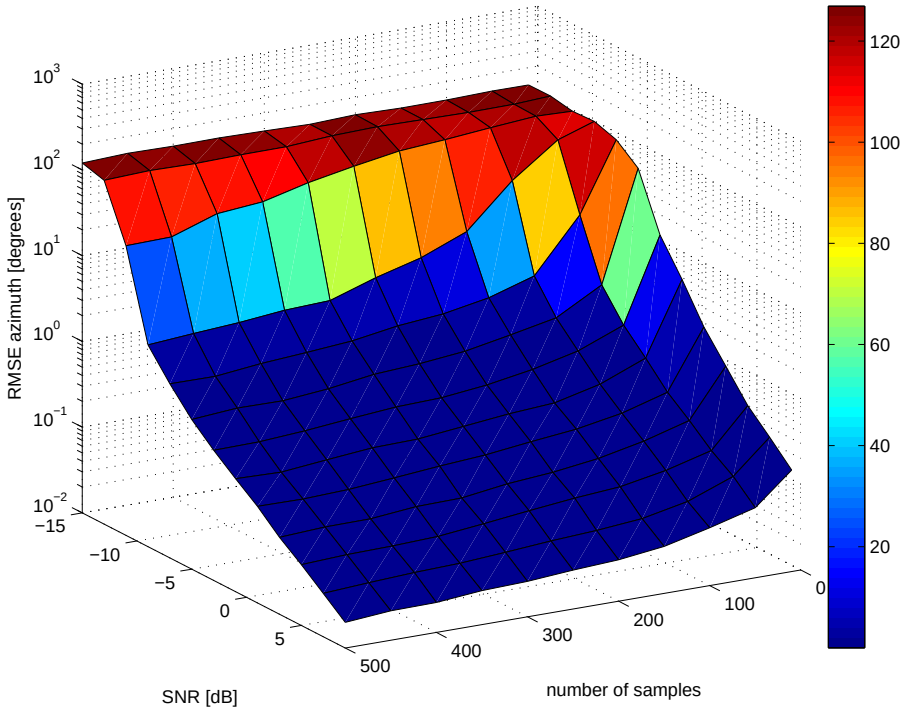

(b)

Figure 5-3: Effect of the number of samples and signal-to-noise ratio on the azimuth estimation error for (a) 9 elements and (b) 17 elements

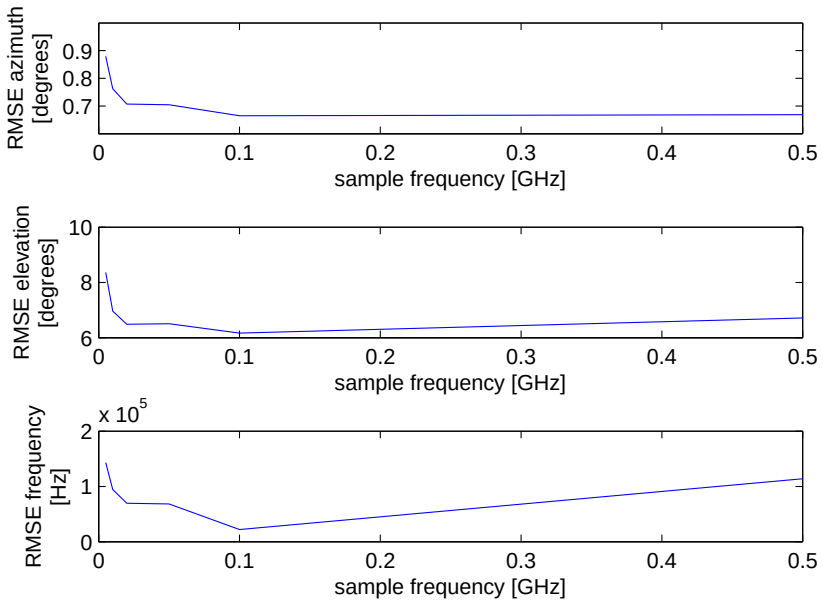

Figure 5-4: RMSE for different samples rate and constant number of sample

samples per period, a short part of one period can be sampled with N samples or some sample frequency between those frequencies can be chosen.
The DOA estimation in the described JAFE-algorithm is based on the phase differences between the particular antenna elements and does not depend on the sample frequency according to the model. At every time the phase differences between the antenna elements are the same if the frequency of a signal does not change. The sample period influences the validity of the narrowband assumption.

Figure 5-4 compares the performance of both algorithms for different ratios between the sample frequency and sample period varying from a sample frequency of 10, 100 and 1000 MHz with a constant number of 1000 samples. This is done by measuring the RMSE for a 1000 test runs. The following parameters are used for every test run: $M = 18$, $N = 100$, $\lambda = 1$, $\beta = 1$, $\theta = 70$ degrees, $\phi = 10$ degrees, $f = 0.1$ GHz, $f_s = 1$ GHz, $SNR = 1$ dB, no spatial smoothing is used and the temporal smoothing factor $m = 10$. Here the chosen elevation is not 90 degrees, because this is a maximum and wrong estimates that are higher than this maximum results in imaginary values, which have no physical meaning. Because an elevation of 70 degrees is chosen the error can result in both smaller and bigger elevation angles.

5-3-2 Conclusion

For low sample frequencies the RMSE of the azimuth, elevation and frequency is high and it reduces fast when the sample frequency is increased. The azimuth error becomes stable at a certain point, but the error of the elevation and especially the frequency increases after the sample rate is increased to a certain amount of oversampling. The big RMSE for the azimuth, elevation and frequency at the beginning is because of the low sample frequency. When the

sample frequency is low many symbol periods of the QPSK-signals are sampled. A temporal smoothing factor of $m = 10$ is used, so according to 4-82 the m consecutive samples of the signal should approximately be the same. For very low frequencies this is not true, so the assumption used in this part of the algorithm is not correct. For higher sample frequencies the RMSE of the elevation and frequency increases. When only a small part of the signal periods is sampled the sample sequences contain multiple samples of more or less the same phase. In that case it is harder to estimate the right frequency when there is noise. This is similar to the reason that a bigger aperture is better for DOA estimation.

Chapter 6

Improved Transformation with Interpolation

Swingler and Davies described a technique for uniform circular arrays that uses extrapolation which mitigates the neglecting of the virtual elements where the Bessel weighting factors are more or less zero [35]. In this chapter I describe how linear interpolation between the physical elements of the circular array can improve the azimuth estimation. Due to this interpolation the data matrix represents a data matrix of the same sized antenna array with more elements. This chapter explains a similar technique to reduce the bias of the phase-mode excitation transformation.
The correctness of the transformation depends on the number of antennas, the spacing between the antennas and the number of phase modes. One can compensate for the errors introduced by the beamspace transformation as is described in [30]. A disadvantage is that it costs extra computations and the technique assumes one fixed elevation for received signal. The Bessel-function approaches zero faster when the wavenumber, k, is small [36]. This is because the argument in the Bessel-function gets smaller. So for a smaller radius the higher order Bessel-function coefficients approaches zero earlier too. On the other hand it increases the effects of mutual coupling between the antenna elements. A different way to deal with this problem of improper approximations by the Bessel-function is to make up data of virtual antenna elements to form an antenna array of the same size with extra antennas. In this case the virtual antennas are placed between each pair of physical antennas and the all the true and imaginary antennas must be uniformly distributed. This way the spacing between the real antenna elements can still be large enough in order to have a good aperture and not too much effect of mutual coupling. This degree of interpolation must be chosen in order that the obtained number of total, real and interpolated, elements M_u is big enough in order to neglect the terms where l is not zero in formula 3-6. Here u is the factor by which the number of antenna elements, M, is upsampled, so $M_u = uM$. The performance is investigated for a uniform circular antenna array of 5 elements, because this is a small number of antennas and 12 elements, because it is even. The reason that an even number of antennas is chosen for the simulation is because the beamspace transformation is a lot less correct for an even number

of antennas than an odd number of antennas. This characteristic is discussed in chapter 5. As Belloni and Koivunen [30] show in their error analysis of the beamspace transform, the maximum bias occurs at an elevation of 90 degrees. For an interpolation factor of $u = 1, 2, 5$ and 10 the RMSE of the azimuth is shown at an elevation angle of 90 degrees. No noise is added and the antenna element spacing is $\lambda/2$. Figure 6-1 and 6-2 show the results for 5 and 12 elements respectively. For the simulation $N = 100$, $d = 0.5\lambda$, $\beta = 1$, $\theta = 90$ degrees, $f = 100$ Hz, $f_s = 1$ kHz and the temporal smoothing factor $m = 10$. No spatial smoothing is used. From these figures it is clear that upsampling leads to better approximation of the beamspace transform in case 5 or 12 elements are used.

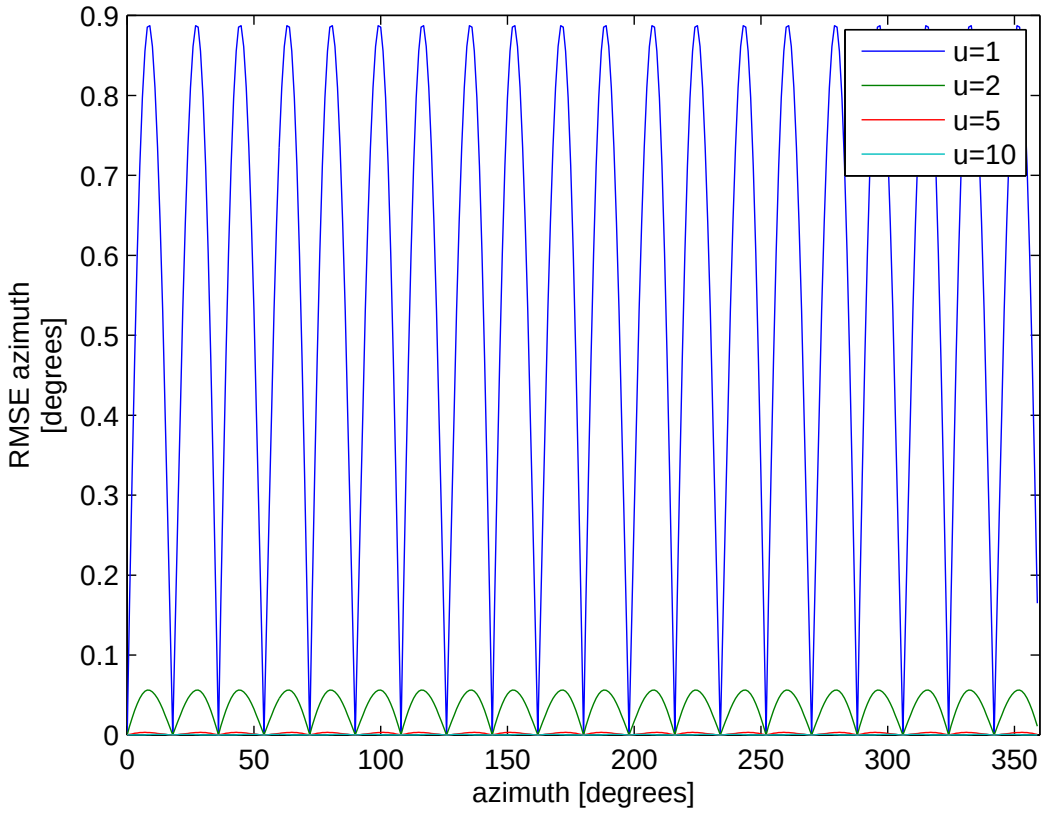

Figure 6-1: RMSE of azimuth after interpolation for an array of 5 elements

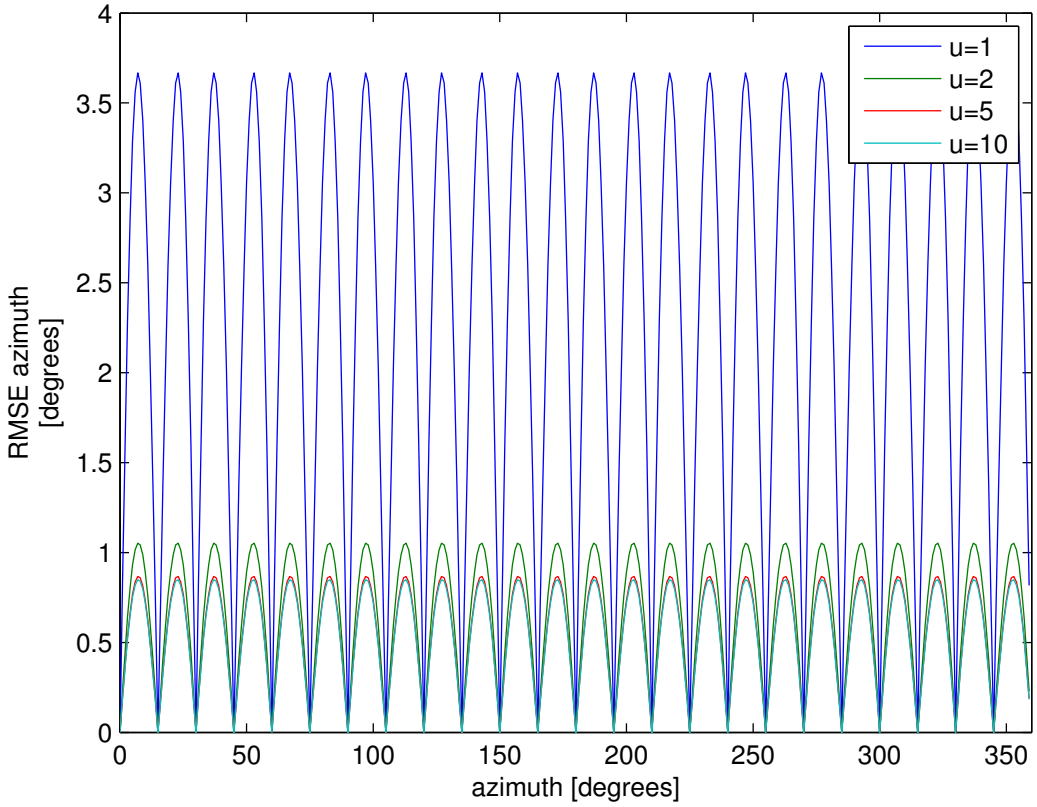

Figure 6-2: RMSE of azimuth after interpolation for an array of 12 elements

Chapter 7

Solutions for Rank Deficiency

Subspace based algorithms use a singular value (or eigenvalue) decomposition to separate the signals from noise. This results in a high resolution, but causes some instabilities. When the azimuth and elevation of two or more signals is the same the array responses are linearly dependent on each other. In case the array responses of two or more signals are linearly dependent or the frequency of two or more signals is the same the data matrix is rank deficient. Then the signal subspace is too small and not all parameters can be estimated correctly.

7-1 Signals With Similar DOAs

Temporal smoothing is frequently used in DOA estimation. When the narrowband assumption is valid it can restore the rank of the data matrix in case multiple signals with different frequencies are coming from the same direction. The time-shift between the stacked matrices causes different phase-shifts for different frequencies. Therefore the stacked array manifolds A_m can elevate the linear dependency between the array manifolds.

The maximum number of sources with different frequencies, but with the same DOA that can be separated from the noise is equal to the amount of stacked matrices, the temporal smoothing factor [27]. It also strengthens the array manifold vectors compared to the zero-mean Gaussian noise vectors. It also makes it possible to estimate the parameters of more sources than antennas at once.

7-2 Signals With Similar Carrier Frequencies

In case of multipath propagation multiple rays of the source signal arrive at different angles at the array. Besides the DOA there is probably also a difference in the power and the delay between all the copies of the signal. In other cases different sources use the same frequency.

For example in UMTS (Universal Mobile Telecommunications System), where CDMA (Code Division Multiple Access) is used. Another situation that can occur is that two cell phone users transmit signals to different base stations and use the same channel. In this situation the signals carry different data symbols and probably have different codes too. Therefore they are not coherent, but they are correlated.

7-2-1 Long Time Sampling

The signals described in chapter 2 are narrowband. Therefore when the frequencies are the same the signals are very much correlated with each other. But in case the signals are not narrowband and the sampled signals represent data sequences with a lot of different symbols, the correlation is not very high. Because of this the data matrix used for the SVD is not rank deficient. But when the narrowband assumption does not hold true the following relationship is not correct.

$$\bar{s}(t-\tau) \approx \bar{s}(t) \tag{7-1}$$

where $\bar{s}$ is the baseband signal. This means that baseband signals change in the time they impinge on the first and last antenna. Therefore the the phase-shift between the antennas is not just defined by the frequency and delay, but also by the baseband signal which cannot be predicted. Thus errors in the DOA estimation will occur. Depending on how correct the narrowband asumption is these errors may be small. To achieve that the data sequences contain a lot of symbols a low sample rate may be required. A problem in electronic warfare is that nothing is known about the signals. So it is hard to decide what sampling time is required for the rank to restore, especially since this is not the same for every signal. Depending on the baud rate it can take a long time and the signals can not be considered as narrowband since the sample frequency approaches the baud rate. It is necessary to sample at least at twice the (intermediate) frequency of the signal, so this technique may result in a large wide data matrix. To cope with this problem it is possible to take periodically two samples at the nyquist rate to achieve 'time' doublets instead of 'antenna' doublets as is required for ESPRIT.

7-2-2 Spatial Smoothing and Forward/Backward Smoothing

Spatial Smoothing is commonly referred to in research papers about uniform linear arrays and also in some papers about uniform circular arrays [3]. This technique cannot be applied on uniform circular arrays directly, because it can only be applied on arrays that have a Vandermonde structure, such as uniform linear arrays. Mathews and Zoltowski described a real beamspace method that uses phase-mode excitation to transform the array structure [2]. With phase-mode excitation the array manifold of the uniform circular array can be transformed to a virtual linear array manifold. Then spatial smoothing and forward/backward smoothing can be applied. A disadvantage of this technique is that it requires the elevation angle to be the same for all angles and to be known or chosen.

Below, the principle of spatial smoothing is explained. This is the similar to what A.N. Lemma described in "ESPRIT based on Joint Angle-Frequency Estimation: Algorithms and Simulations" for uniform linear arrays [3]. The spatial smoothed data matrix is constructed by stacking L submatrices horizontally. These submatrices consist of $M_L = M - L + 1$ rows.

$$X_L = [J_1 X \; J_2 X \; \dots J_L X] \tag{7-2}$$

where

$$J_i = [0_{i-1} \; I_{M_L} \; 0_{L-i}] \tag{7-3}$$

where 0_q is a matrix consisting of q columns with zeros. The array manifolds in A_ζ have a shift invariance structure:

$$\mathbf{a}_\zeta(\phi) = \begin{bmatrix} e^{-jP\phi} \\ \vdots \\ 1 \\ \vdots \\ e^{jP\phi} \end{bmatrix} \tag{7-4}$$

So the value of every element is the product of the value above and $e^{j\phi}$. Due to this shift invariance property the following relation is true:

$$J_i A_\zeta = J_1 A_\zeta \Phi^{i-1} = A'_\zeta \Phi^{i-1} \tag{7-5}$$

where

$$\Phi = \begin{bmatrix} e^{j\phi_1} & & & \\ & e^{j\phi_2} & & \\ & & \ddots & \\ & & & e^{j\phi_d} \end{bmatrix} \tag{7-6}$$

Then X_L has the following form:

$$X_L = A'_\zeta [F_s \; \Phi F_s \; \dots \; \Phi^{L-1} F_s] \tag{7-7}$$

where A'_ζ are the first $M - L + 1$ rows of A_ζ and F_s is described in equation 4-78.

7-3 Evaluation of Temporal and Spatial Smoothing

In this section the angular and frequency resolution is investigated for the 1-D DOA JAFE-algorithm. Usually algorithms that use the singular value or eigenvalue decomposition deteriorate when the DOAs of multiple signals are the same or when the frequencies are similar. The singular value decomposition separates the data into orthogonal signal subspace components. When two or more DOAs or frequencies are the same, the data matrix is not full rank. This results in a wrong signal subspace. In case two or more signal sequences are correlated the resulting signal subspace is also affected. To prevent this rank loss spatial and temporal smoothing is used. The effect on the accuracy of the estimates is investigated.

7-3-1 Effect of Temporal Smoothing on Closely Spaced Azimuth Angles

To cope with the problems of closely spaced DOAs temporal smoothing is used. In this section the performance improvement is shown in case temporal smoothing is used. The joint angle-frequency estimation that is used has standard temporal smoothing of a factor of $m \geq 2$ to obtain temporal samples in the columns. This is used for frequency estimation. This section shows the improvements when a temporal smoothing factor higher than 2 is used.

First the resolution is investigated by estimating the DOAs of two signals for separations from 0 to 8 degrees. The spacing between the angles will have some effect on the mean of the estimates. Therefore not just the RMSE is computed, but both the mean and the standard deviation of the estimates. Besides the effect of the separation between the two signals on the mean and standard deviations also the effect of noise on the estimation performance is investigated. In this case the mean and standard deviation are computed for the same reason as for the error due to the angle separation. Since both signals have their own standard deviations the combined standard deviations are in both situations computed by averaging the variances of both azimuth estimates.

The first simulation is performed with two signals without modulation, one with a frequency of 0.1 kHz and one with a frequency of 0.2 kHz. The elevation for both signals is 90 degrees. The number of antenna elements is 9 and the antenna spacing is 0.42λ. The number of samples is 100, $d = 0.42\lambda$ and the sample frequency is 1 kHz. The SNR is 1 dB and the signal separation goes from 0 degrees to 8 degrees. The result is given in figure 7-1 and 7-2. For the simulation 1000 Monte Carlo simulations are performed.

When two signals are closely spaced the singular value decomposition results in one big component and a small one which may have a singular value in the order of the noise. When temporal smoothing is applied the singular values of the signals get bigger, which makes it possible to separate both signal components from the noise. The noise in the vectors that are stacked is in this simulations zero-mean Gaussian and independent and identically distributed (i.i.d.) and because of this the singular values of the noise components are not increased when the noise samples are stacked. In reality this i.i.d can usually not be assumed if the sample frequency is very high, because then the adjacent noise samples are correlated due to physical effects which are not included in the model. Therefore the singular value decomposition can separate the closely spaced signals. This causes the singular value decomposition to give output vectors with a better signal-to-noise ratio. This section investigates the resolution

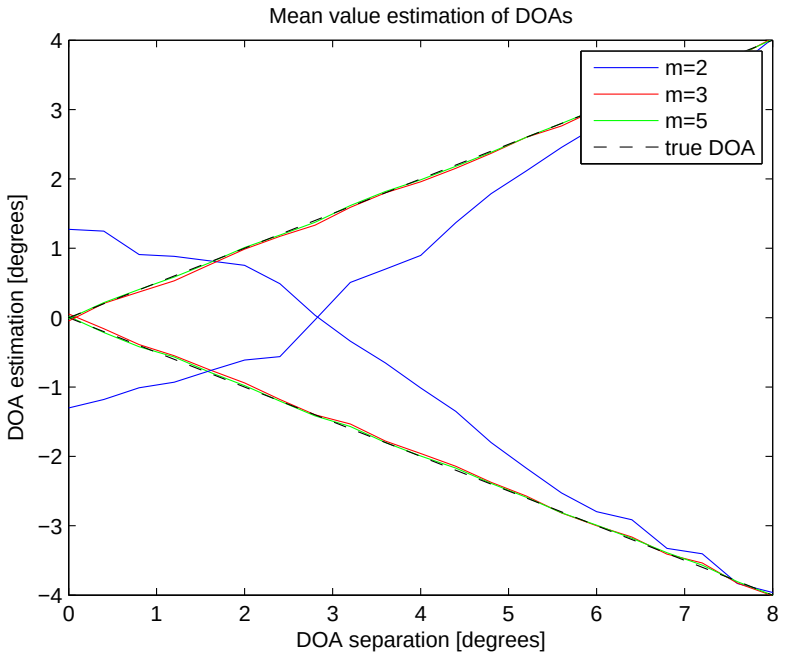

Figure 7-1: Mean of DOA estimation

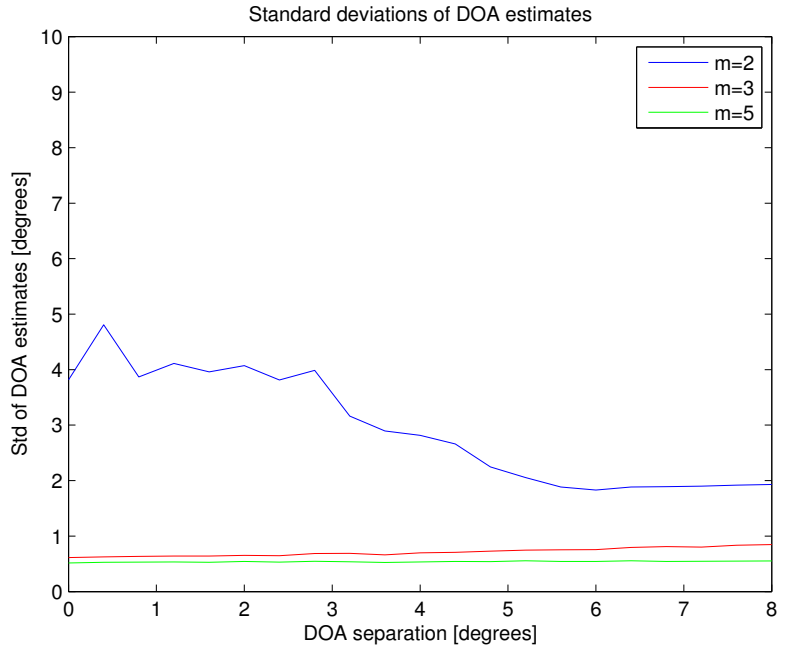

Figure 7-2: Standard deviation of DOA estimation

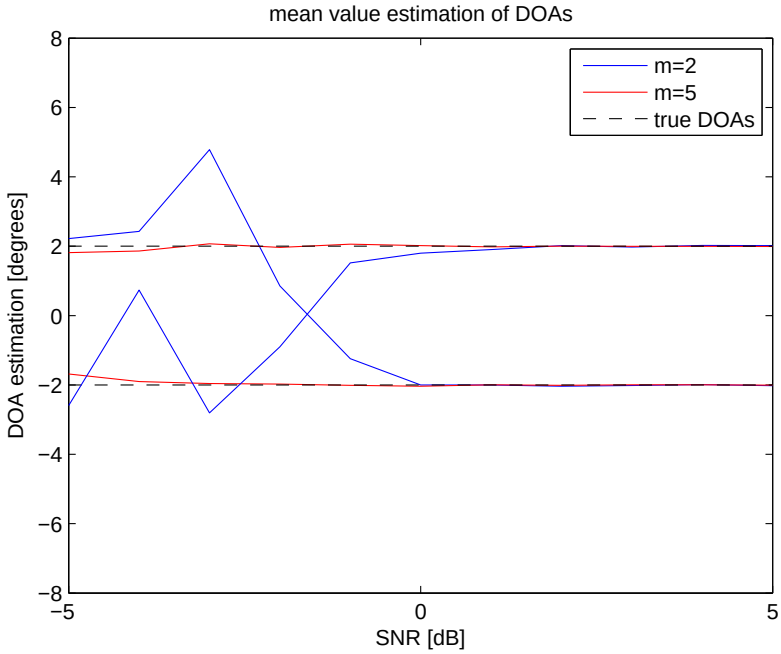

Figure 7-3: Mean estimate of closely spaced angles for varying SNR

in case of different signal-to-noise ratios. For the simulation the following parameters are used:$M = 15$, $N = 100$, $d = 0.42\lambda$, $\beta_1 = \beta_2 = 1$, $\theta_1 = \theta_2 = 90$ degrees, $f = 100$ Hz and $f_s = 1$ kHz.

Figures 7-1 and 7-2 show that temporal smoothing helps in case the DOAs of the signals are close to each other. The temporal smoothing factor that is required for the algorithm to work properly depends on the number of signals that are closely spaced. For a DOA separation of 7 degrees or more and a temporal smoothing factor of $m = 2$, the mean estimation is very close to the true azimuth angles, but the standard deviation is more than 2 degrees. A temporal factor of $m = 3$ or $m = 5$ reduces the standard deviation and makes it possible to estimate the azimuth angles without a bias when the separation is small. A higher temporal smoothing factor has no influence on the mean azimuth estimation, but reduces the standard deviation a little bit. The blue lines in figure 7-1 crosses each other. Since the estimated DOAs belong to a certain frequency it is for sure that which DOA estimate belongs to which true DOA even if it is closer to the other one. Therefore this is an effect of the algorithm.

The blue line in figures 7-3 and 7-4 represents the azimuth estimation in case a temporal factor of $m = 2$ is used and shows the performance deteriorates below a SNR of 0 dB. Figure 7-4 shows that the SNR has a lower bound on the performance in this case for a temporal factor $m = 2$ at circa -2 dB.

7-3-2 Effect of Spatial Smoothing on Correlated Signals

With spatial smoothing, defined in section 7-2-2, it is possible to separate correlated signals as well as coherent signals. The smoothing factor has influence on how many coherent signals can be separated, but more smoothing than necessary also decorrelates the signals more,

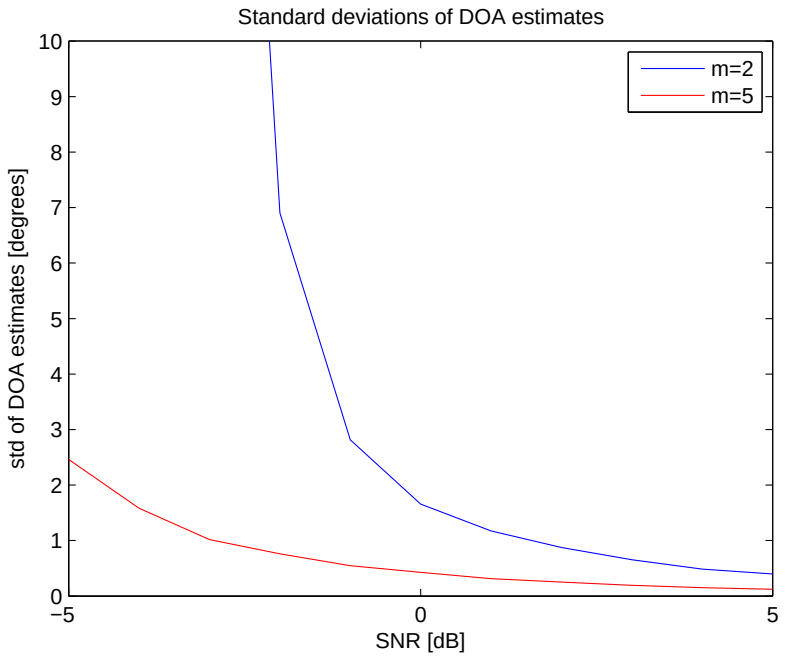

Figure 7-4: Standard deviation estimate of closely spaced angles for varying SNR

which leads to more accurate separation. On the other hand, spatial smoothing does decrease the aperture of the antenna array and thus the resolution. This section shows when spatial smoothing technique [3] works and when not with the 1-D DOA JAFE-algorithm for the uniform circular array.

The following simulations show the effect of spatial smoothing on the RMSE of the azimuth estimation of two correlated signals. The simulation is performed with different smoothing factors in order to show it works and to show how more smoothing contributes to the decorrelation of the signals. A spatial smoothing factor of $L = 1$ indicates that the array is divided into 1 subarray which means no spatial smoothing. Notice that the smoothing factor also defines the maximum number of coherent signals that can be separated theoretically. The following parameters are used: $M = 9$, $N = 500$, $d = 0.5\lambda$, $SNR = -5$ dB, $\beta_1 = \beta_2 = 1$, $\theta_1 = \theta_2 = 90$ degrees, $\phi_1 = 10$, $\phi_2 = 90$ degrees, $f_s = 1$ kHz and the temporal smoothing factor $t = 10$.

Figure 7-5 shows that spatial smoothing helps when the carrier frequencies of different signals approach each other. A spatial smoothing factor $L \geq 2$ is necessary for proper estimation. More spatial smoothing than necessary results in a smaller standard deviation as can be seen in figure 7-6.

7-3-3 Conclusion

This section shows how temporal and spatial smoothing can be applied to uniform circular arrays and how it can contribute in certain scenarios. For linear arrays this was already

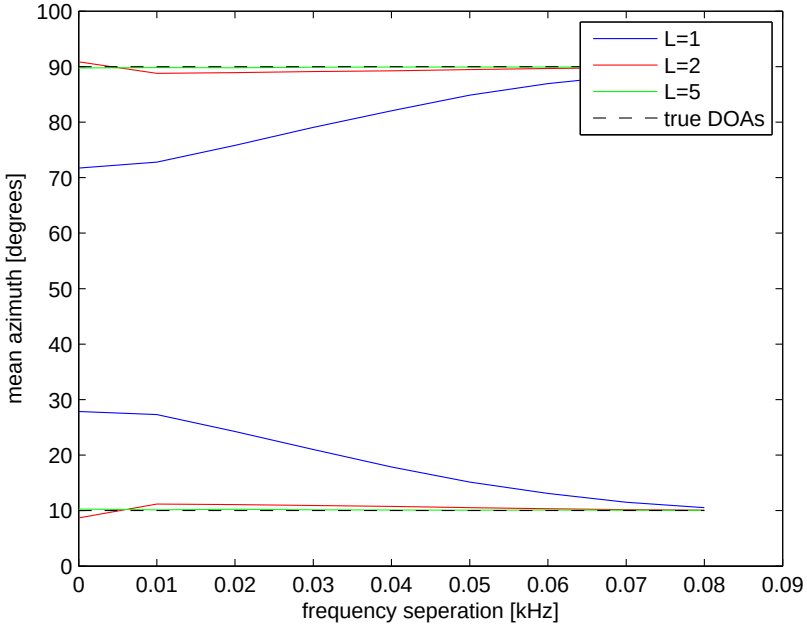

Figure 7-5: Mean of DOA estimation

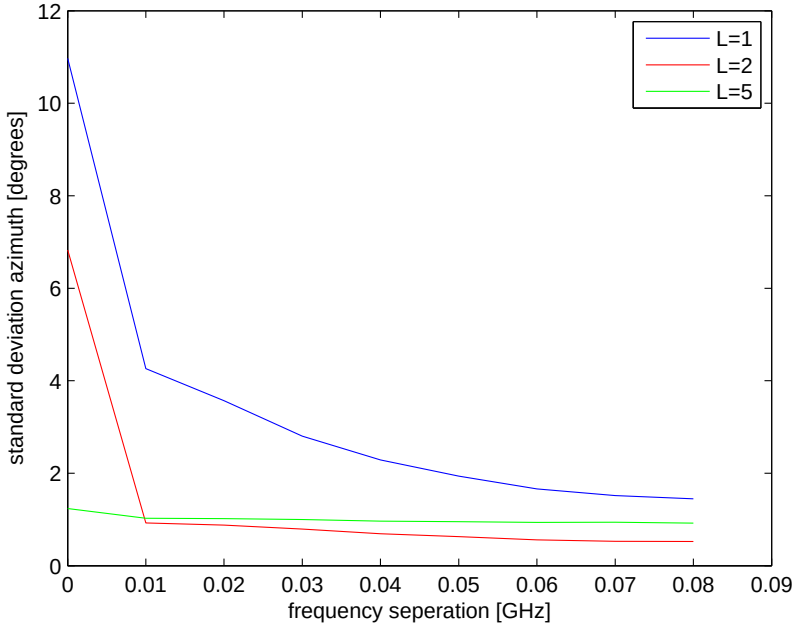

Figure 7-6: Standard deviation of DOA estimation

demonstrated by [3]. The temporal smoothing factor must be at least the same as the number of the maximum closely spaced signals at the same direction. More temporal smoothing makes the algorithm able to still separate closely spaced azimuth angles in noisy environments.
Spatial smoothing is necessary for proper mean azimuth estimation when the carrier frequencies of two different signals are close to each other or the same. More spatial smoothing leads to a smaller standard deviation in case the signals have the same frequency, but leads to a slightly higher standard deviation when the frequencies are not the same, but almost the same. The reason for this must be the reduced aperture.

Chapter 8

Additional Options with ESPRIT-based JAFE-algorithm

.

8-1 Joint Angle-Frequency-Delay Estimation

In case of multipath propagation it can be advantageous to find the delays between the multipath rays. This can be used for better detection of the symbols as is done with a RAKE receiver or the information of the delays can be used to get information about the environment or location of the transmitter.

8-1-1 Data Model

The model described in chapter 2 has to be extended so that it contains the time delays between the signals. The following model is used to represent r multipath rays of one signal that impinge on the antenna array.

$$\mathbf{x}(t) = \sum_{i=1}^{r} \mathbf{a}(\theta_i, \phi_1)[\delta(\tau_i) * \mathbf{s_1}(t)] \tag{8-1}$$

where $\mathbf{s}$ represents the down-converted signals, which are time-shifted copies of each other, $\delta(\tau)$ represents the kronecker delta pulse and r is the number of multipath rays.

8-1-2 Blind Signal Separation

To estimate the delays between the multipath components the signals must be separated. Then one signal can be used as reference signal for the others. After ESPRIT for linear arrays on the transformed circular array data matrix is performed for DOA estimation, signal separation is not very hard. The SVD already separated the signal subspace from the noise subspace. The signal subspace appears in the columns of U_s and V_s with singular values Σ_s. The columns of U_s and V_s are a combination of the columns of the array manifolds and the signals:

$$\begin{aligned} X_s &= U_s \Sigma_s V_s = A T^{-1} \Sigma_s T S && \text{(8-2)} \\ U_s &= A T^{-1} && \text{(8-3)} \\ V_s &= T S && \text{(8-4)} \\ & && \text{(8-5)} \end{aligned}$$

where X_s is an estimation of the data matrix by removing the noise with the singular value decomposition and Σ_s is a diagonal matrix with the singular values of the signals on the diagonal. With ESPRIT the parameters of the DOAs can be estimated from U_s by dividing the upper part by the lower part of this matrix and performing an eigenvalue decomposition on the result. Then the eigenvalues contain the DOA information and the obtained eigenvectors form the T matrix. This can be used along with Σ_s to obtain an estimation $\hat{S}$ of the signal.

$$\hat{S} = T^{-1} V_s \tag{8-6}$$

Then the first row can be used as reference for estimating the delay of the other signals.

8-1-3 Delay Estimation with ESPRIT

This chapter describes how the delay can be estimated using an ESPRIT technique. It is assumed that only one signal is present which arrives at the array via multiple reflections. The different rays have different path lengths from source to array, which causes the delay. To estimate the signals with an ESPRIT technique the signals has to be transformed to the frequency domain. By applying a digital Fourier transform (DFT) to that data a time delay translates to a phase shift [37]:

$$\tilde{S} = \hat{S} F \tag{8-7}$$

where

$$F = \begin{bmatrix} 1 & 1 & 1 & 1 \\ 1 & \gamma & \dots & \gamma^{N-1} \\ 1 & \gamma^2 & & \\ 1 & \vdots & & \vdots \\ 1 & \gamma^{N-1} & \dots & \gamma^{(N-1)^2} \end{bmatrix} \tag{8-8}$$

with $\gamma = e^{-j2\pi/N}$. The columns of $\tilde{S}$ represent the multipath rays 1 to r of one source:

$$\tilde{S} = \begin{bmatrix} \tilde{\mathbf{s}}_1 \\ \tilde{\mathbf{s}}_2 \\ \vdots \\ \tilde{\mathbf{s}}_r \end{bmatrix} \tag{8-9}$$

where $\tilde{\mathbf{s}}_i$ is a row vector containing the N samples of the ith signal. Since the signal is not known one of the rays has to be chosen as a reference signal, for example the first. The other signals are then delayed versions of the reference and in the Fourier domain this delay is described as follows:

$$\tilde{\mathbf{s}}_i = \tilde{\mathbf{s}}_1 e^{-j2\pi f \tau_i} = \tilde{\mathbf{s}}_1 \gamma_i^{\tau_i N} \tag{8-10}$$

By multiplying the signals with the pseudo-inverse of the reference signal a vector with the following shift invariance structure is obtained. This technique is based on a similar technique used in [37]:

$$\tilde{\mathbf{s}_1}^{\dagger} \odot \tilde{\mathbf{s}_i} = Z_i = [\gamma_i^{\tau_i 1} \ \gamma_i^{\tau_i 2} \ \dots \ \gamma_i^{\tau_i N}] \tag{8-11}$$

where $\odot$ is a point wise multiplication of the elements. By selecting the first $N-1$ elements and the last $N-1$ elements and multiplying the first vector with the pseudo-inverse of the other vector the phase shift is obtained with a ESPRIT technique. From the phase-shift the delay can be computed as follows:

$$Z_{x,i}^{\dagger} Z_{y,i} = \gamma_i^{\tau_i} \tag{8-12}$$

where

$$Z_{x,i} = Z_i[I_{N-1}\ \mathbf{0}_1] \tag{8-13}$$
$$Z_{y,i} = Z_i[\mathbf{0}_1\ I_{N-1}] \tag{8-14}$$

From the phase-shift the delay τ_i can be computed as follows:

$$\tau_i = \log(\gamma_i^{\tau_i})\frac{N}{-j2\pi} \tag{8-15}$$

8-1-4 Simulation

When two signals are transformed to the frequency domain and one of them is a delayed version of the other it results in the same Fourier transform except for a phase shift. The first sample of the data of the delayed version are not present in the reference signal, because this part of the data data arrived earlier in the reference signal. Because of this the two are not just delayed versions of each other, but contain some different samples. Therefore the Fourier transforms are not exactly the same, but as long as only a few samples differ this only causes a small error. The simulations in this chapter are performed with the following parameters: $M = 18$, $N = 375$, $\beta_1 = \beta_2 = 1$, $d = 0.42\lambda$, $\theta_1 = \theta_2 = 90$ degrees, $\phi_1 = 10$ degrees, $\phi_2 = 130$ degrees, $f = 8$ kHz, $f_s = 100$ kHz and the symbols rate is 0.8 kHz. No temporal and spatial smoothing is used. For the first simulation signal pulses are used to test if the theory works. Figure 8-1 shows an example of the received pulses with a delay of 2 µs.

In figure 8-2 it can be seen that the SNR must be very high to obtain reasonable results, which is unrealistic. The problem can either occur at the signal separation or the algorithm, but it is clear that the SNR has a big influence. The first step of the signal separation is performed by separating the signal subspace from the noise with the singular value decomposition. Figure 8-3 shows the first 7 singular values for the case that two multipath rays are received from an azimuth angle of 10 and 130 degrees. No spatial or temporal smoothing is used. The first two singular values represent the singular values that belong to the signals and the other singular values belong to the noise. When there is no noise the first singular value, which belongs to the first vector, should be big and the second a bit smaller, depending on the amount of dependency on the first vector. Just as in figure 8-2 the result is very good for SNRs of 40 dB or higher. For SNRs lower than 40 dB the noise has more impact on the result. Then the signal subspace is not a perfect mixture of the signals, but is changed a little bit by the noise. A little bit of noise apparently causes the algorithm to fail. One of the reasons for this is that a lot of noise outside the pulse period is taken into account and another reason is that the delays are very small and therefore the effect of the noise dominates.

8-1-5 Further Research

There are two possibilities to improve the estimation of the delays with ESPRIT. The first possibility is to improve the signal separation. In case the SNR is not very high the signal

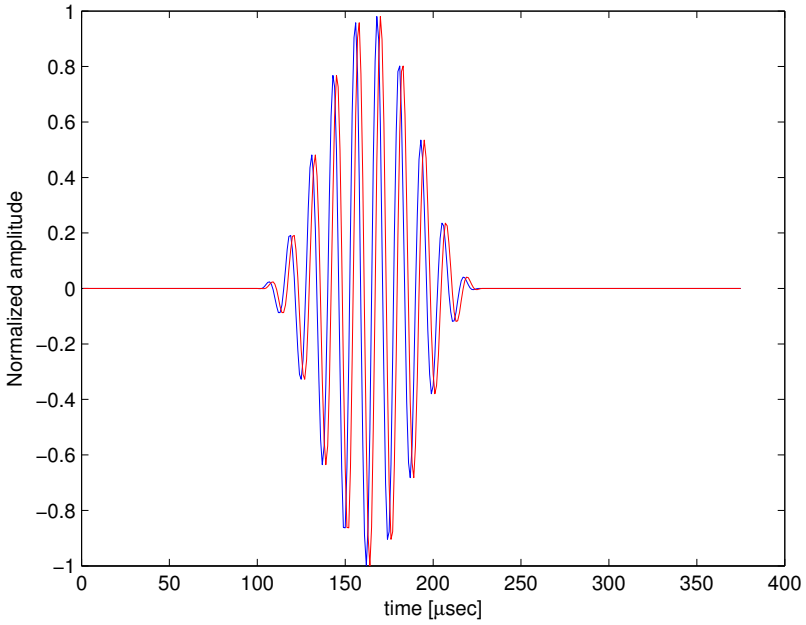

Figure 8-1: Signal pulses

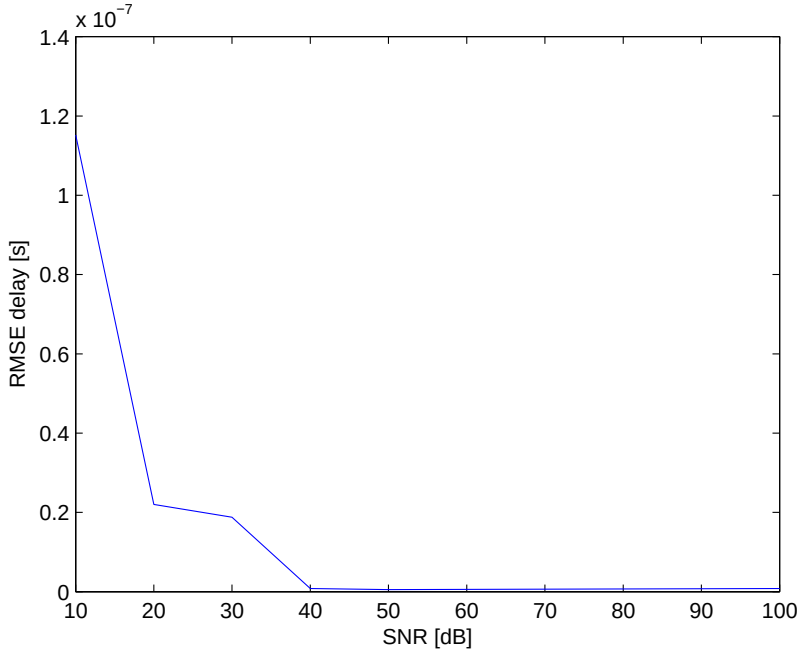

Figure 8-2: RMSE of delay estimation when pulses are used

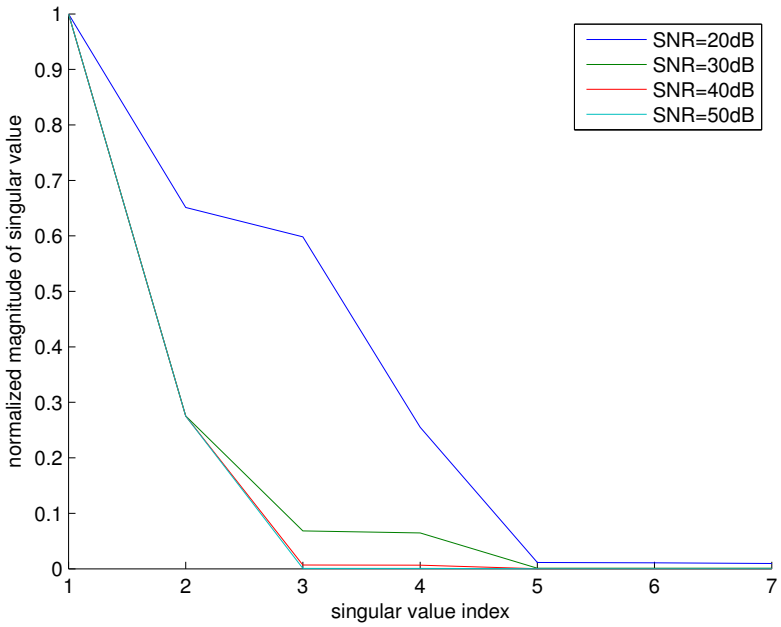

Figure 8-3: Singular values of signal ans noise vectors

subspace obtained from the singular value decomposition is not perfect, which causes the algorithm to fail. So the signal separation can be improved by adding structure to the data matrix or using a different technique for signal separation. The second possibility is to improve the algorithm to estimate the delay when the signals are not perfect. In case delay estimation based on the Fourier transform is used, as in the before presented ESPRIT algorithm, the correctness on the Fourier transformed model for noisy and imperfect signals must be checked.

Chapter 9

Conclusions and Recommendations

In this chapter the conclusions and recommendations of this research project are presented. The research objectives and the results of the research are described. Then the scientific contributions are presented, which is followed by the recommendations.

9-1 Conclusions

Information about radio communication in an environment is of interest in electronic warfare. With antenna array processing joint angle-frequencies can be estimated. The objective of this research project is to design an algorithm that can be used for joint angle-frequency estimation in electronic warfare scenarios with a circular antenna array. A circular antenna array can, due to its 2D geometry, estimate the azimuth angle from 0 to 360 degrees without ambiguities plus the elevation. Other geometries that span a planar array can be used to estimate the DOA of signals 360 degrees around the array, but for some purposes the circular geometry can be advantageous. An advantage of a uniform circular antenna array is that when one wants to cope with mutual coupling uniform antenna arrays are more convenient [1]. There is no hard constraint on the number of antenna elements, but it is preferred the algorithm gives good results with a number of antennas between 5 and 10. Furthermore the algorithm must be able to estimate signals with low SNR, singals that are coherent and signals with similar DOAs.
To achieve this objective the following approach is used. First the possible solutions and existing algorithms are described. Then an algorithm is chosen and extended for coherent signals and a technique to improve the algorithm in case few antenna elements are used is given in chapter 6. After that the performance is investigated for different numbers of antenna elements, different SNRs and different sample rates is given. This is followed by a investigation of the effects of temporal and spatial smoothing for JAFE with a circular array. Finally the possibilities for an extension of the algorithm for joint angle-frequency-delay estimation is investigated.
As algorithm for the uniform circular array an ESPRIT based algorithm is chosen for its

high resolution and efficiency. ESPRIT requires a Vandermonde structure and therefore the beamspace transform is applied to the data to transform the structure of the uniform circular array to the proper structure for the shift-invariance technique. Pre-processing is required for ESPRIT to make it suitable for the estimation of coherent signals. When all signals have the same elevation, this elevation can be chosen to transform the manifold to the structure necessary for spatial smoothing. The spatial smoothing technique is tested by simulating the RMSE azimuth error in case of two coherent signals and noise. From the simulation results it can be seen that in case of two coherent signals a spatial smoothing factor of two is required, but a higher factor reduces the standard deviation of the RMSE of the azimuth angles. In case of signals with slightly different frequencies a higher spatial smoothing factor than necessary is a little bit worse. In case multiple signals have the same DOA or closely spaced DOAs the algorithm cannot estimate the right joint frequencies, but simulations demonstrate that temporal smoothing make it possible to estimate signals with the same azimuth angle. A higher temporal smoothing factor than two reduces the standard deviation and is necessary for estimating two closely spaced azimuth angles in case of low SNRs. With temporal smoothing it is also possible to estimate more sources than antennas. One of the constraints was that the algorithm should perform well in case few antenna elements are used. Simulations show that the number of elements has large effect on the systematic error in the azimuth estimation caused by the beamspace transform. An even number of elements is causing a much larger systematic error than an odd number of elements. When 5 elements are used the bias in the azimuth estimation can reach up to almost 0.9 degrees, which may be too much for some purposes. Spatial interpolation of the data matrix of the circular array can reduce this bias to circa 0.05 degrees when the number of 5 elements is interpolated to 10 elements as is described in chapter 6. For an even number of antenna elements the same principle is demonstrated with a circular array of 12 elements. For 12 elements the systematic error of the azimuth estimation reaches up to 3.7 degrees. With interpolation this error can be reduced to a little bit less than 1 degrees.
Besides the DOA and frequency signals possess more parameters. In case of multipath propagation the delays between the multipath rays can be estimated. The algorithm can be extended with the estimation of the delay with the ESPRIT technique. It is necessary to separate the signals first, since nothing about the signals is known on forehand, and then use the Fourier transform to obtain the required shift-invariance structure with delay information. Simulations show that when the signals are not recovered perfectly, which happens when the SNR is not very high, the algorithms fails.

9-2 Scientific Contributions

This section points out the scientific contribution made in this thesis

- A JAFE-algorithm that can estimate the azimuth angles and frequencies of signals using the linear ESPRIT variant on a circular array which can estimate correlated and coherent signals as well as signals from the same direction is described in section 4-2 and section 7-3-2.
- The performance of a JAFE-algorithm that uses an ESPRIT-based algorithm for a uniform circular array is simulated for varying numbers of elements, samples and SNRs;

- The effects of spatial and temporal smoothing on the estimation of the azimuth and frequency of signals with almost similar DOAs and frequencies is investigated;
- The effect of the sample rate on the RMSE of the azimuth, elevation and frequency is shown in simulations where QPSK-symbols are used.
- The possibility of a joint angle-frequency-delay algorithm with ESPRIT are described and problems of this technique for low SNR are demonstrated;
- It is demonstrated that improvement of the beamspace transform for uniform circular arrays is possible by linear spatial interpolation of the array before applying the transform.

9-3 Recommendations

The following recommendations can be made, based on the results of this thesis.

- For the data model the signals are assumed to be narrowband. Research could how the algorithm must be modified to be able to estimate broad and/or wideband signals.
- Antennas could break down or be out of position. Research should show if the algorithm can cope with broken antenna elements and antenna misplacements.
- When the circular array manifold is transformed to a linear array manifold with a Vandermonde structure by fixing the elevation at 90 degrees it is assumed all sources are in the plane of the array. The effect of sources, that are not exactly in that plane, on the angle estimation error should be investigated.
- The spatial interpolation technique, used for reducing the systematic error induced by the beamspace transform, works well for 5 elements, but for an even number of 12 elements the error is reduced, but it is still almost 1 degrees. Smarter interpolation techniques may reduces the systematic error more.
- The computational efficiency of the algorithm could probably be improved.
- ESPRIT is dependent on the array geometry and requires a calibrated array. Research on techniques that make it possible to use ESPRIT with uncalibrated arrays could lead algorithms that are more practical to use.
- Circular arrays are advantageous when compensating for mutual coupling [1]. The influence of this compensating on the algorithms described in this thesis could be investigated.
- The model used in this thesis assumes a uniform circular array consisting of isotropic antennas. Isotropic antennas are a theoretical concept and do not exist in reality. The algorithm for 1-D DOA estimation could use omnidirectional antennas as well if it is only used in environments where signals in the plane of the array are to be estimated. Research on the performance of the algorithm with omnidirectional antennas could show a more realistic image of the performance of the algorithm.

Appendix A

Simulation

The Monte Carlo simulations in this thesis are performed in MATLAB. The signals are complex sinusoidal signals unless mentioned otherwise. In all simulations complex white Gaussian noise is added to the signal received on a particular antenna element.

A-1 Signal Types

The easiest way to construct a signal is just implementing a complex harmonic signal of a certain frequency. After the signals is sampled noise is added. Figure A-1 represents such a signal with frequency 20 kHz, sample frequency 500 kHz, 1000 samples and a signal-to-noise ratio of 10 dB.

In some cases it is interesting to see what happens to the result of some algorithm when some kind of modulation technique is applied. Figure A-2 represents a QPSK-signal with a carrier frequency of 2 kHz, sample frequency 500 kHz, 1000 samples and a signal-to-noise ratio of 10 dB is depicted.

Figure A-3 depicts some samples of 100 QPSK data symbols for signal-to-noise ratios of 5 and 10 dB.

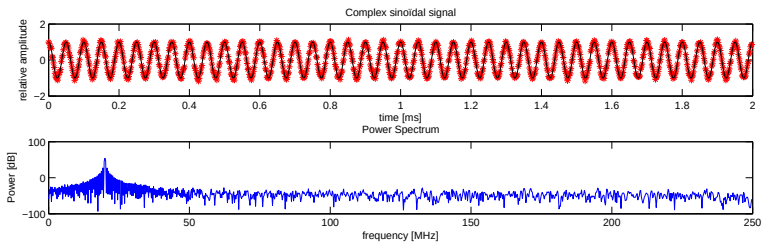

Figure A-1: Complex sinusoidal signal

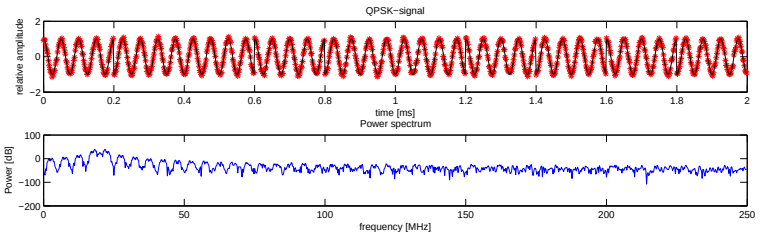

Figure A-2: QPSK-signal

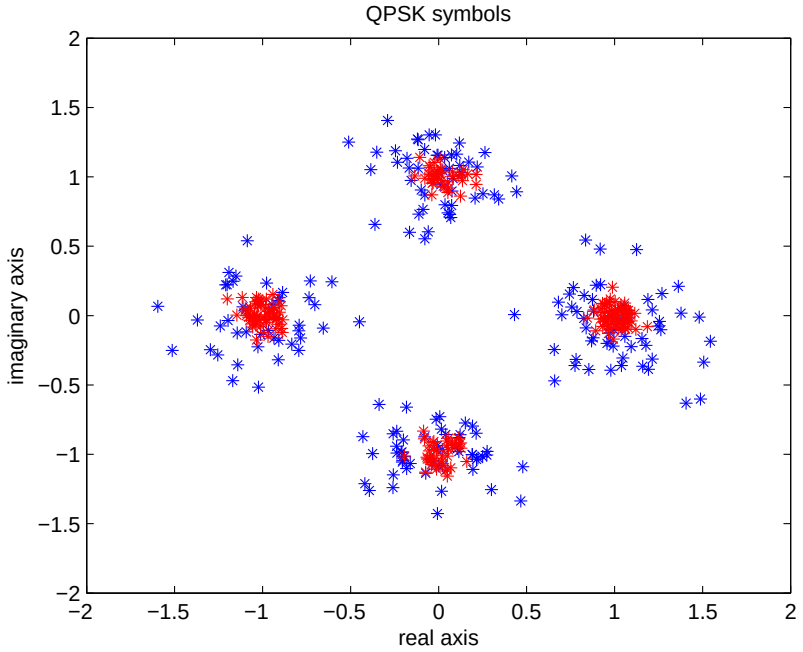

Figure A-3: QPSK symbols

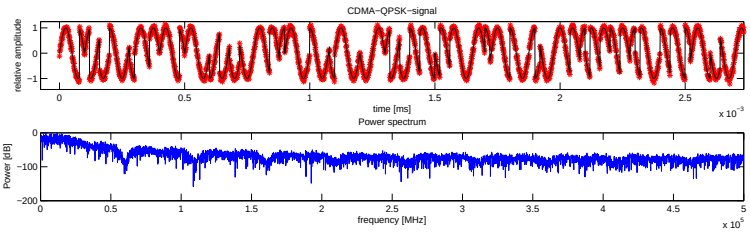

Figure A-4: a single CDMA-QPSK signal

Figure A-4 depicts a single CDMA signal with QPSK modulation. The CDMA code has 16 random bits of $+1$ and -1 of which the sum equals zero. From the power spectrum it is clear the frequency is harder to estimate well.

Appendix B

Phase-mode Excitation

This appendix described the technique of phase-mode excitation. It is based on citeHyberg7119,rudge,MPZ94,belloni. In a uniform linear array incoming plane waves arrive with a certain constant time delay between the antenna elements causing a constant phase shift between the antenna elements. This results in the so called Vandermonde structure [27] shown by following equation:

$$\begin{aligned} a_{\text{ULA}} &= [1 \; e^{i2\pi 1\Delta \sin(\phi)} \; e^{i2\pi 2\Delta \sin(\phi)} \; \ldots \; e^{i2\pi (M-1)\Delta \sin(\phi)}]^T && \text{(B-1)} \\ &= [1 \; \psi \; \psi^2 \; \ldots \; \psi^{M-1}]^T && \text{(B-2)} \end{aligned}$$

where Δ is the spacing between the antennas in wavelengths. This special structure is used in algorithms as ESPRIT (Estimation of signal parameters via rotation invariance techniques). Unfortunately the array manifold of a uniform circular array is not of this form. A way to restore this form is with the theory of phase-mode excitation [38].

First of all the array manifold can be expressed as a Bessel function [39] with help of the following mathematical formula:

$$e^{z\frac{t-t^{-1}}{2}} = \sum_{q=-\infty}^{\infty} t^q J_q(iz) \tag{B-3}$$

If t is replaced by ju the following equation is obtained:

$$e^{jz\frac{u+u^{-1}}{2}} = \sum_{q=-\infty}^{\infty} j^q u^q J_q(iz) \tag{B-4}$$

When the cosinus part in the equation of the array manifold of a uniform circular array is written in exponentials this equation can be used to express the array manifold of this kind of array in Bessel functions [28]. By letting $z = kr\sin(\theta)$ and $u = e^{\phi-\phi_m}$ the following equation results for the mth array element:

$$a_{\mathrm{UCA,m}}(\theta,\phi) = e^{jkr\sin(\theta)\cos(\phi-\phi_m)} = e^{jkr\sin(\theta)\frac{e^{j(\phi-\phi_m)}+e^{-j(\phi-\phi_m)}}{2}} \tag{B-5}$$

$$= \sum_{q=-\infty}^{\infty} j^q J_q(kr\sin(\theta))e^{jq(\phi-\phi_m)} \tag{B-6}$$

$$= \sum_{q=-\infty}^{\infty} j^q J_q(kr\sin(\theta))e^{jq(\phi-2\pi\frac{m}{M})} \tag{B-7}$$

The subscript m denotes the specific antenna element and $\phi_m = 2\pi\frac{m}{M}$. Since circular arrays are continuous the array manifold can be expressed as a periodic function with a period of 2π. Therefore array manifold can be represented in terms of a complex Fourier series. The Fourier series of a function $f(x) \in L^2([-\pi,\pi])$ has the form

$$f_m = \sum_{p=-\infty}^{\infty} c_p e^{jp2\pi\frac{m}{M}} \tag{B-8}$$

$$c_p = \frac{1}{M}\sum_{m=0}^{M-1} f_m e^{-jp2\pi\frac{m}{M}} \tag{B-9}$$

In this case of a uniform circular array the function f_m is replaced by $a_{UCA,m}(\theta,\phi)$. The Fourier Series of the array manifold is the sum of an infinite number of phase-modes p [28]:

$$a_{\mathrm{UCA,m}}(\theta,\phi) = \sum_{p=-\infty}^{\infty} a_p(\theta,\phi)e^{-jp2\pi\frac{m}{M}} \tag{B-10}$$

In this equation the Fourier Coefficients $a_p(\theta,\phi)$ are given by

$$a_p(\theta,\phi) = \frac{1}{M}\sum_{m=0}^{M-1} a_{\mathrm{UCA,m}}(\theta,\phi)e^{j2\pi\frac{m}{M}p} \tag{B-11}$$

$$= \frac{1}{M}\sum_{m=0}^{M-1}\sum_{q=-\infty}^{\infty} j^q J_q(kr\sin(\theta))e^{jq(\phi-2\pi\frac{m}{M})}e^{j2\pi\frac{m}{M}p} \tag{B-12}$$

$$= \frac{1}{M}\sum_{q=-\infty}^{\infty} j^q J_q(kr\sin(\theta))e^{jq\phi}\sum_{m=1}^{M} e^{j2\pi\frac{m}{M}(p-q)} \tag{B-13}$$

The last sum equals M in case the difference between p and q is M times an integer; $q-p = Ml$ where l is an integer. Otherwise it is zero, because the complex numbers over the unity circle cancel each other out. Therefore instead of the sum over all values of q the sum of l integers from $-\infty$ to ∞ is taken where q is replaced by $p + Ml$. This leads to the following equation [2, 38]:

$$a_p(\theta, \phi) = \sum_{l=-\infty}^{\infty} j^{p+Ml} J_{p+Ml}(kr\sin(\theta)) e^{j(p+Ml)\phi} \tag{B-14}$$

The Bessel function has the property that if the order becomes larger than the argument it decreases. So when $p + Ml$ becomes larger than $krsin(\theta)$, which is less than or equal to kr, the Bessel function decreases. When for example $p = 2$ and $M = 10$ then $p + Ml = 2 + 10l$. This results in $p + Ml = -8$ for $l = -1$, $p + Ml = 2$ for $l = 0$ and $p + Ml = 12$ for $l = 1$. The result of the Bessel function of the case of $l = 0$ dominates over the case $l = -1$ and $l = 1$ and over cases with larger l [2]. So if $M \gg p$ then the l=0-term dominates, so the term for $\neq 0$ can be ignored and the equation becomes:

$$a_p(\theta, \phi) \approx j^p J_p(kr\sin(\theta)) e^{jp\phi} \tag{B-15}$$

An approximation is made by stating that the part of the phase-mode where $l = 0$ dominates over the other parts of the sum. So to achieve a good performance the following assumption must hold:

$$|J_p(kr\sin(\theta))| \gg |J_{p-M}(kr\sin(\theta))| \tag{B-16}$$

When p becomes large the magnitude of the Bessel-function of that order is more or less zero, so can be neglected. The following equation can be used to compute this maximum number of p that cannot be neglected [28, 38] :

$$P = \lfloor kr \rfloor = \lfloor \frac{2\pi r}{\lambda} \rfloor \tag{B-17}$$

This P depends on the wavelength of the signal and the radius of the antenna array. This radius is dependent on the number antenna elements and the spacing between them.

Finally the obtained phase-modes from $-P$ to P form the following beamspace UCA vector:

$$\hat{\mathbf{a}}_{uca} \approx \begin{bmatrix} A_{-P}(\theta, \phi) e^{-jP\phi} \\ \vdots \\ 1 \\ \vdots \\ A_p(\theta, \phi) e^{jP\phi} \end{bmatrix} = \begin{bmatrix} j^{-P} J_{-P}(kr\sin(\theta)) e^{-jP\phi} \\ \vdots \\ J_0(kr\sin(\theta)) \\ \vdots \\ j^P J_P(kr\sin(\theta)) e^{jP\phi} \end{bmatrix} \tag{B-18}$$

Bibliography

[1] R. Goossens and H. Rogier, "2-d direction-of-arrival estimation in the presence of mutual coupling by exploiting the symmetry in a uniform circular array," in *Antennas and Propagation Society International Symposium, 2007 IEEE*, pp. 5283–5286, June 2007.

[2] C. P. Mathews and M. Zoltowski, "Eigenstructure techniques for 2-d angle estimation with uniform circular arrays," *Signal Processing, IEEE Transactions on*, vol. 42, no. 9, pp. 2395–2407, 1994.

[3] A. N. Lemma, *ESPRIT based on Joint Angle-Frequency Estimation: Algorithms and Simulations*. PhD thesis, Delft University of Technology, 2000.

[4] T.-J. Shan, M. Wax, and T. Kailath, "On spatial smoothing for direction-of-arrival estimation of coherent signals," *Acoustics, Speech and Signal Processing, IEEE Transactions on*, vol. 33, pp. 806–811, Aug 1985.

[5] H. Krim and M. Viberg, "Two decades of array signal processing research: the parametric approach," *Signal Processing Magazine, IEEE*, vol. 13, no. 4, pp. 67–94, 1996.

[6] T. Gunasekaran and K. S. KUMAR, "Modified concentric circular microstrip array configurations for wimax base stations.," *Journal of Theoretical & Applied Information Technology*, vol. 12, 2010.

[7] T. Fu, S. Jin, and X. Gao, "Joint 2-d angle and frequency estimation for uniform circular array," in *Communications, Circuits and Systems Proceedings, 2006 International Conference on*, vol. 1, pp. 230–233, 2006.

[8] C. Hui and W. Yongliang, "A modified method of frequency and 2-d angle estimation," in *Antennas and Propagation Society International Symposium, 2003. IEEE*, vol. 3, pp. 920–923 vol.3, June 2003.

[9] R. Roy, A. Paulraj, and T. Kailath, "Esprit–a subspace rotation approach to estimation of parameters of cisoids in noise," *Acoustics, Speech and Signal Processing, IEEE Transactions on*, vol. 34, pp. 1340–1342, Oct 1986.

[10] R. Roy and T. Kailath, "Esprit-estimation of signal parameters via rotational invariance techniques," *Acoustics, Speech and Signal Processing, IEEE Transactions on*, vol. 37, pp. 984–995, Jul 1989.

[11] J. T. P. Cherntanomwong and H. Tsuji, "Reduction of aoa estimation error due to perturbation in array response by spatial smoothing preprocessing,"

[12] M. Zoltowski, M. Haardt, and C. P. Mathews, "Closed-form 2-d angle estimation with rectangular arrays in element space or beamspace via unitary esprit," *Signal Processing, IEEE Transactions on*, vol. 44, pp. 316–328, Feb 1996.

[13] C. El Kassis, J. Picheral, G. Fleury, and C. Mokbel, "Direction of arrival estimation using em-esprit with nonuniform arrays," *Circuits, Systems, and Signal Processing*, vol. 31, no. 5, pp. 1787–1807, 2012.

[14] A. Lemma, A.-J. van der Veen, and E. Deprettere, "Joint angle-frequency estimation using multi-resolution esprit," in *Acoustics, Speech and Signal Processing, 1998. Proceedings of the 1998 IEEE International Conference on*, vol. 4, pp. 1957–1960 vol.4, May 1998.

[15] J. Liang and D. Liu, "Joint elevation and azimuth direction finding using l-shaped array," *Antennas and Propagation, IEEE Transactions on*, vol. 58, pp. 2136–2141, June 2010.

[16] T. Fu, S. Jin, and X. Gao, "Joint 2-d angle and frequency estimation for uniform circular array," in *Communications, Circuits and Systems Proceedings, 2006 International Conference on*, vol. 1, pp. 230–233, June 2006.

[17] R. Goossens and H. Rogier, "2-d angle estimation with spherical arrays for scalar fields by means of unitary spherical esprit," in *Antennas and Propagation Society International Symposium, 2009. APSURSI '09. IEEE*, pp. 1–4, June 2009.

[18] S. Akkar, F. Harabi, and A. Gharsallah, "Concentric circular array for doas estimation of coherent sources with esprit algorithm," in *Design and Technology of Integrated Systems in Nanoscale Era (DTIS), 2010 5th International Conference on*, pp. 1–6, March 2010.

[19] C. Hui, W. Yongliang, and W. Zhiwen, "Frequency and 2-d angle estimation based on uniform circular array," in *Phased Array Systems and Technology, 2003. IEEE International Symposium on*, pp. 547–552, Oct 2003.

[20] H. Yi, H. Hu, Z. Zhou, and X. Zhang, "Spc12-3: Cumulant-based jafe algorithm in spatially and temporally correlated gaussian noise," in *IEEE Globecom 2006*, pp. 1–5, 2006.

[21] M. Feng and K. D. Kammeyer, "Suppression of gaussian noise using cumulants: a quantitative analysis," in *Acoustics, Speech, and Signal Processing, 1997. ICASSP-97., 1997 IEEE International Conference on*, vol. 5, pp. 3813–3816 vol.5, Apr 1997.

[22] J. E. Evans, D. Sun, and J. Johnson, "Application of advanced signal processing techniques to angle of arrival estimation in atc navigation and surveillance systems," tech. rep., DTIC Document, 1982.

[23] I. Longstaff, P. E. K. Chow, and D. E. N. Davies, "Directional properties of circular arrays," *Electrical Engineers, Proceedings of the Institution of*, vol. 114, pp. 713–718, June 1967.

[24] M. Zoltowski and C. P. Mathews, "Direction finding with uniform circular arrays via phase mode excitation and beamspace root-music," in *Acoustics, Speech, and Signal Processing, 1992. ICASSP-92., 1992 IEEE International Conference on*, vol. 5, pp. 245–248 vol.5, Mar 1992.

[25] C. A. Balanis, *Antenna Theory: Analysis and Design*. Wiley-Interscience, 2005.

[26] H. Landau, "Sampling, data transmission, and the nyquist rate," *Proceedings of the IEEE*, vol. 55, pp. 1701–1706, Oct 1967.

[27] A. Lemma, A.-J. van der Veen, and E. Deprettere, "Analysis of joint angle-frequency estimation using esprit," *Signal Processing, IEEE Transactions on*, vol. 51, no. 5, pp. 1264–1283, 2003.

[28] P. Hyberg, *Antenna array mapping for DOA estimation in radio signal reconnaissance*. PhD thesis, KTH, Signal Processing, 2005. QC 20101022.

[29] K. A. Al Jabr, *Modified UCA-ESPRIT and modified UCA-ROOT-MUSIC for estimating DOA of coherent signals using one snapshot*. PhD thesis, Wichita State University, 2007.

[30] F. Belloni and V. Koivunen, "Beamspace transform for uca: Error analysis and bias reduction," *Signal Processing, IEEE Transactions on*, vol. 54, pp. 3078–3089, Aug 2006.

[31] M. Zoltowski and C. P. Mathews, "Closed-form 2d angle estimation with uniform circular array via phase mode excitation and esprit," in *Signals, Systems and Computers, 1993. 1993 Conference Record of The Twenty-Seventh Asilomar Conference on*, pp. 169–173 vol.1, Nov 1993.

[32] H. Minghao, Y. Yixin, and Z. Xianda, "Uca-esprit algorithm for 2-d angle estimation," in *Signal Processing Proceedings, 2000. WCCC-ICSP 2000. 5th International Conference on*, vol. 1, pp. 437–440 vol.1, 2000.

[33] C. Tan, P. Fletcher, M. Beach, A. Nix, M. Landmann, R. Thoma, *et al.*, "On the application of circular arrays in direction finding. part i: Investigation into the estimation algorithms," 2002.

[34] S. Burintramart and T. Sarkar, "Target localization in three dimensions," *Advances in Direction of Arrival Estimation*, 2005.

[35] D. Swingler and S. Davies, "Spatial harmonic interpolation and extrapolation for use with circular arrays," in *Communications, Computers and Signal Processing, 1991., IEEE Pacific Rim Conference on*, pp. 138–141 vol.1, May 1991.

[36] C. Gentile, A. J. Braga, and A. Kik, "A comprehensive evaluation of joint range and angle estimation in ultra-wideband location systems for indoors," in *Communications, 2008. ICC'08. IEEE International Conference on*, pp. 4219–4225, IEEE, 2008.

[37] A.-J. van der Veen, M. Vanderveen, and A. Paulraj, "Joint angle and delay estimation using shift-invariance techniques," *Signal Processing, IEEE Transactions on*, vol. 46, pp. 405–418, Feb 1998.

[38] A. Rudge, *The Handbook of Antenna Design Vol. 2*. Peter Peregrinus Ltd., London, UK., 1983.

[39] M. Kreh, "Bessel functions," *Lecture Notes, Penn State - Göttingen Summer School on Number Theory*, 2012.

Glossary

List of Acronyms

ESPRIT Estimation of Signal Parameters via Rotational Invariance Techniques

MVDR Minimum Variance Distortionless Response

MUSIC Multiple SIgnal Classification

DOA Direction-of-Arrival

JAFE Joint Angle-Frequency Estimation

MLE Maximum Likelihood Estimation

UCA Uniform Circular Array

ULA Uniform Linear Array

SNR Signal-to-Noise Ratio

RMSE Root-Mean-Square Error

std standard deviation

CDMA Code Division Multiple Access

BPSK Binary Phase Shift Keying

QPSK Quadrature Phase Shift Keying

List of Symbols

M Number of antenna elements

N Number of samples

θ Elevation(degrees)

ϕ Azimuth (degrees)

M_p Number of phase modes

p Phase-mode number

P Maximum phase mode

λ Wavelength (m)

τ Delay (s)

r Received signal

$\bar{r}$ Complex envelope

s Received down-converted signal

$\bar{s}$ Complex envelope of down-converted signal

f_c Carrier frequency (Hz)

f Intermediate frequency (Hz)

f_s Sample frequency (Hz)

B Observed bandwidth (Hz)

W Signal bandwidth (Hz)

r Radius (m)

d Antenna spacing (m)

k Wavenumber (radians/m)

$\mathbf{a}$ Array manifold

T_s Sampling time (s)

m Temporal smoothing factor

L Spatial smoothing factor

J_q Bessel function of qth orher

u Spatial upsampling factor